

AD-A203 401

2

REPORT NO. NADC-88078-60



**SYNTHESIS PROCESSING OF
HIGH-LITHIUM Al-Li ALLOYS**

Dr. John Wert
University of Virginia
Charlottesville, VA 22901

27 JUNE 1988

Progress Report
62234N/RS34A57/1/ZP180

Public Release: Distribution Unlimited

Prepared for
AIRBORNE MATERIALS BLOCK
Department of the Navy
Warminster, PA 18974

DTIC
ELECTE
S JAN 6 1989 D
eb H

DISTRIBUTION STATEMENT A
Approved for public release.
Distribution Unlimited

89 1 06 026

REPORT DOCUMENTATION PAGE

1a. REPORT SECURITY CLASSIFICATION Unclassified		1b. RESTRICTIVE MARKINGS		
2a. SECURITY CLASSIFICATION AUTHORITY		3. DISTRIBUTION / AVAILABILITY OF REPORT Approved for public release; Distribution is unlimited.		
2b. DECLASSIFICATION / DOWNGRADING SCHEDULE				
4. PERFORMING ORGANIZATION REPORT NUMBER(S) NADC-88078-60		5. MONITORING ORGANIZATION REPORT NUMBER(S) N/A		
6a. NAME OF PERFORMING ORGANIZATION University of Virginia	6b. OFFICE SYMBOL <i>(If applicable)</i>	7a. NAME OF MONITORING ORGANIZATION N/A		
6c. ADDRESS (City, State, and ZIP Code) Charlottesville, VA 22901		7b. ADDRESS (City, State, and ZIP Code) N/A		
8a. NAME OF FUNDING / SPONSORING ORGANIZATION Naval Air Development Center	8b. OFFICE SYMBOL <i>(If applicable)</i> 6063	9. PROCUREMENT INSTRUMENT IDENTIFICATION NUMBER N62269-86-C-0253		
8c. ADDRESS (City, State, and ZIP Code) Warminster, PA 18974-5000		10. SOURCE OF FUNDING NUMBERS		
		PROGRAM ELEMENT NO. 62234N	PROJECT NO. RS34A57	TASK NO. 1
11. TITLE (Include Security Classification) Synthesis Processing of High-Lithium Al-Li Alloys				
12. PERSONAL AUTHOR(S) Dr. John Wert				
13a. TYPE OF REPORT Progress	13b. TIME COVERED FROM 7/8/86 TO 4/30/88	14. DATE OF REPORT (Year, Month, Day) 27 June 88	15. PAGE COUNT	
16. SUPPLEMENTARY NOTATION				
17. COSATI CODES		18. SUBJECT TERMS (Continue on reverse if necessary and identify by block number) Rapid Solidification, Aluminum, Lithium		
FIELD	GROUP			SUB-GROUP
11	06			
11	06.01			
19. ABSTRACT (Continue on reverse if necessary and identify by block number) <p>The goal of this research project is to determine the feasibility of producing Al-Li-base alloys suitable for structural applications with densities in the range 2.2 to 2.4 Mg/m³. Alloys belonging to two broad categories have been studied thus far: Al-Li-Mg alloys and Al-Li-(Y, Sb) alloys. The alloy compositions were selected to avoid formation of the AlLi phase which has deleterious effects on mechanical and electrochemical properties when a substantial volume fraction is present. Rapid solidification has been used to retain a fine microstructure, since all of the alloys exceeded the solubility limit. Splat-quenched flakes of several compositions within each category have been studied, both as-quenched and after an annealing treatment designed to simulate hot vacuum degassing. After annealing, the Al-Li-Mg alloys contained the Al₂LiMg phase in equilibrium with an Al matrix. The Al-Li-Mg flakes exhibit a ductile fracture mechanism when the volume fraction of Al₂LiMg is less than 0.25. The microstructures of the Al-Li-(Y,Sb) alloys are more complex and do not appear as promising for further development. Based on the studies of the splat-quenched flakes, an Al-5.6Li-9.8Mg extrusion has been prepared and preliminary results are presented.</p>				
20. DISTRIBUTION / AVAILABILITY OF ABSTRACT <input type="checkbox"/> UNCLASSIFIED/UNLIMITED <input checked="" type="checkbox"/> SAME AS RPT <input type="checkbox"/> DTIC USERS		21. ABSTRACT SECURITY CLASSIFICATION Unclassified		
22a. NAME OF RESPONSIBLE INDIVIDUAL Dr. William E. Frazier		22b. TELEPHONE (Include Area Code) 215-441-1301	22c. OFFICE SYMBOL 6063	

FOREWORD

The following progress report describes work performed on Navy Contract No. N62269-86-C-0253, "Synthesis Processing of High-Lithium Al-Li Alloys". The work accomplished and reported herein was performed by University of Virginia, Charlottesville, Virginia 22901. The program was monitored by Dr. William E. Frazier of the Naval Air Development Center, Aerospace Materials Division, Warminster, PA.



Accession For	
NTIS GRA&I	<input checked="" type="checkbox"/>
DTIC TAB	<input type="checkbox"/>
Unannounced	<input type="checkbox"/>
Justification	
By _____	
Distribution/	
Availability Codes	
Dist	Avail and/or Special
A-1	

NADC 88078-60

TABLE OF CONTENTS

1. INTRODUCTION	1
2. BACKGROUND	3
2.1 Rapid Solidification Processing	3
2.1.1 Characteristics of Rapid Solidification	3
2.1.2 Production of Rapidly Solidified Material	4
2.1.3 Consolidation of the RS Particles	4
2.1.4 Application of RS Processing to Al-Li Alloys	4
2.2 Development of (Sub)grain Structure During Extrusion ..	8
2.2.1 Relaxation Processes	8
2.2.2 Influence of Microstructure on Relaxation During Extrusion	9
2.2.3 Influence of Processing Conditions	10
2.3 Structure and Properties of RSP Al-Li Alloys	11
2.3.1 Grain Structure	11
2.3.2 Oxide Particles	11
2.3.3 Constituent Particles	12
2.3.4 RSP Al-Li Alloys Incorporating Dispersoid-Forming Elements	13
2.3.5 RSP Al-Li Alloys Incorporating Precipitate-Forming Elements	14
2.3.6 Mechanical Properties: Influence of Processing Conditions and Oxide Particles	15
2.3.7 Mechanical Properties: Influence of Composite Precipitates or Dispersoids	16
2.3.8 Mechanical Properties: RSP Al-Li Alloys Incorporating Precipitate-Forming Elements	17
2.3.8.1 Influence of Grain/Subgrain Structure	17
2.3.8.2 Influence of Mg Addition	17
2.3.8.3 Influence of Cu Addition	17
2.3.8.4 Influence of the Amount of Li	18
2.3.8.5 Influence of Constituent Particles	18
2.4 Stabilization of the Al_3Li Phase	19
2.4.1 Structure of A_3B Compounds	19
2.4.2 Factors Affecting Intermetallic Crystal Structure and Stability	19
2.4.3 Application to Stabilization of Al_3Li Phase	22
2.5 Al-Li-Mg Alloy System	27
3. EXPERIMENTAL PROCEDURE	30
3.1 Materials and Heat-Treatment	30
3.2 Microstructural Characterization	30
3.3 Property Characterization	31

4. EXPERIMENTAL RESULTS	33
4.1 Characterization of the Materials	33
4.2 Study of the Al-Li-Mg Flakes	34
4.2.1 RS Microstructure	34
4.2.2 Annealed Microstructure	34
4.2.3 Deformation Characteristics of Flakes	39
4.2.3.1 Fracture Surface of Annealed Flakes	39
4.2.3.2 Micro-Hardness Measurements	41
4.3 Study of the Al-Li-Y Flakes	44
4.3.1 Rapidly-Solidified Microstructure	44
4.3.2 Annealed Microstructure	44
4.4 Study of the Al-Li-Sb Flakes	50
4.5 Microstructure of the Melt-Spun Consolidated Al-Li-Mg Alloy	55
5. FUTURE WORK	59
6. REFERENCES	60
7. APPENDIX	64

LIST OF FIGURES

Fig. 1 Consolidation procedure for RS particles, schematic of the alloy particle oxide. (After Kim, Griffith and Froes) 5

Fig. 2 Schematic effect of temperature, pressure and strain rate on the allowable working range. (After Dieter) .. 7

Fig. 3 Atomic structure on close-packed layers in: (a) T-type ordered structure, and (b) R-type ordered structure. (After Liu) 20

Fig. 4 Aluminum-Lithium phase diagram. Dashed lines represent metastable Al_3Li solvus. (After Flower and Gregson) 23

Fig. 5 Binary trialuminide compounds with structures indicated as a function of electronegativity difference and radius ratio. 25

Fig. 6 Isothermal section of the Al-Li-Mg ternary phase diagram at $400^{\circ}C$. (After Levinson and McPherson) 29

Fig. 7 TEM micrographs of as-splat quenched Al-Li-Mg flakes. 35

Fig. 8 Optical micrographs of as-splat quenched Al-Li-Mg flakes. 36

Fig. 9 Dark field TEM micrograph showing Al_3Li precipitates in an as-splat quenched Al-Li-Mg flake. 37

Fig. 10 Optical micrographs of annealed Al-Li-Mg flakes. ... 38

Fig. 11 TEM micrographs of annealed Al-Li-Mg flakes. 40

Fig. 12 SEM micrographs showing the fracture surfaces of annealed Al-Li-Mg flakes. 42

Fig. 13 DPH microhardness of the Al-Li-Mg flakes. 43

Fig. 14 Optical micrographs of as-splat quenched Al-Li-Y flakes. 45

Fig. 15 TEM micrographs of as-splat quenched Al-Li-Y flakes. 46

Fig. 16 Optical micrographs of Al-Li-Y flakes annealed for 2 hours at $300^{\circ}C$ 47

Fig. 17 TEM micrographs of Al-Li-Y flakes annealed for 2 hours at $300^{\circ}C$ 49

NADC 88078-60

Fig. 18	TEM micrographs of as-splat quenched Al-Li-Sb flakes.	51
Fig. 19	TEM micrographs of Al-Li-Sb flakes annealed for 2 hours at 300°C.	52
Fig. 20	Optical micrographs of as-splat quenched Al-Li-Sb flakes.	53
Fig. 21	Optical micrographs of Al-Li-Sb flakes annealed for 2 hours at 300°C.	54
Fig. 22	Optical micrographs of Al-5.65Li-9.8Mg melt-spun ribbon.	56
Fig. 23	Optical micrographs showing the L, S and T sections of the Al-5.65Li-9.8Mg extruded bar.	57
Fig. 24	TEM micrographs showing a longitudinal section of the Al-5.65Li-9.8Mg extruded bar.	58

1. INTRODUCTION

The goal of this research program is to demonstrate the feasibility of producing Al-Li-base alloys suitable for structural applications, with densities 15 to 20 percent lower than 7075 Al. The alloy compositions being investigated contain 4 to 5 wt% lithium, more than can be taken into solid solution in aluminum. These alloys cannot employ precipitation-hardening as a primary strengthening mechanism, in contrast to Al-Li-Cu and Al-Li-Cu-Mg alloys nearing commercial introduction. As a consequence of the elevated lithium level; the strength, ductility, toughness and corrosion resistance will have different relationships to alloy composition and processing conditions than precipitation-strengthened Al-Li-base alloys. Consideration of the novel processing-microstructure-property interrelationships raises several fundamental questions about Al-Li-base alloys with elevated lithium levels, questions that are being answered in the current research project. Critical fundamental questions are:

- Can formation of coarse primary phases be avoided during solidification and processing, especially AlLi phase?
- Can processing methods be identified that produce a stable substructure which contributes substantially to strength?
- Can alloys of this type provide levels of ductility, toughness and corrosion resistance needed for structural applications?

The remainder of this introductory section briefly outlines the benefits to be gained by elevated lithium additions to aluminum, and the perceived barriers to attaining useful properties in alloys of this type.

When lithium is added to aluminum, the elastic modulus increases by approximately 2% and density decreases by approximately 1% for each atom percent addition up to the solubility limit (1). These benefits are obtained for Li in solid solution or in Al_3Li precipitates. The benefits of decreasing density and increasing elastic modulus produced by adding Li to aluminum have been described by several authors (2,3). Weight reduction from the density decrease provides the largest advantage for most aerospace applications, although the elastic modulus increase is significant for stiffness-critical applications. No other chemical element with appreciable solubility in aluminum produces equivalent effects on the density and elastic modulus (4).

The potential for weight reduction in aerospace structures has driven development of heat-treatable aluminum-lithium alloys by all major aluminum producers in the United States and Europe. Alloys that offer a 7 to 9 percent decrease in density compared to 7075 Al, with service properties similar to conventional high-strength aluminum alloys, are now nearing commercial introduction. Commercialization of these alloys has required a technological solution for the problem of reactivity of aluminum-

lithium alloys during casting, and application of fundamental materials science principles to solve problems of poor ductility and toughness. However, solutions to these problems appear to be attainable, so it is appropriate to consider whether larger reductions in density and increases in elastic modulus may be obtained by larger additions of lithium.

The major barrier to larger lithium additions is formation of AlLi in alloys containing more Li than can be taken into solid solution at elevated temperatures. AlLi is a strongly anodic phase that leads to poor corrosion properties (5-7). Furthermore, coarse AlLi particles degrade ductility and toughness, an undesirable effect in Al-Li-base alloys where toughness is somewhat lower than in conventional precipitation-hardening aluminum alloys (2,3,8).

The restriction that Li not exceed the solubility limit in complex alloys containing several alloying additions places a limit of about 9 percent on the density reduction that can be obtained through addition of lithium to aluminum. However, material technology trade-off studies of the effect of property improvements on structural efficiency clearly show that further density reductions would permit additional structural weight reductions (3). Thus, new types of Al-Li-base alloys containing lithium additions that exceed the solubility limit would find applications, provided that the service properties of the new alloys approached those of conventional precipitation-hardening alloys.

At least 2 technical approaches have the potential to solve the problems associated with lithium levels exceeding the solubility limit. An approach investigated at the Boeing Airplane Company under Air Force sponsorship (9) is retention of lithium in supersaturated solid solution by rapid solidification or mechanical-alloying. The findings of the Boeing program demonstrate that formation of primary phases composed of rapidly-diffusing species such as lithium cannot be prevented during hot consolidation processing. A second approach, synthesis of alloys in which AlLi is replaced by an alternate equilibrium phase that does not produce the deleterious effects of AlLi phase, has not yet been explored in detail. The current research program is investigating the feasibility of this approach by addressing the fundamental questions listed earlier. Alloy compositions investigated include Al-Li-Mg, Al-Li-Y and Al-Li-Sb.

2. BACKGROUND

The alloys being investigated are non heat-treatable, rapid solidification processed (RSP), Al-Li based alloys of high lithium content. The microstructure evolves during rapid solidification and hot compaction and a (sub)grain structure develops during hot extrusion. Thus, it is appropriate to consider our current understanding of the topics of rapid solidification, consolidation processing and of structure or substructure development during extrusion. This background information is covered in sections 2.1 through 2.3, with emphasis on how it may be applied to RSP Al-Li alloys.

Two sets of alloys are being studied. The first set consists of Al-Li-Mg alloys and the second consists of Al-Li-Y and Al-Li-Sb alloys where yttrium and antimony are added in an attempt to stabilize the Al_3Li phase. Sections 2.4 and 2.5, respectively, describe the Al-Li-Mg system and the concepts which were used for the choice of Sb and Y as the Al_3Li stabilizing elements.

2.1 Rapid Solidification Processing

2.1.1 Characteristics of Rapid Solidification

Although most aluminum alloys are still fabricated by the conventional solidification followed by working, it has recently become apparent that rapid solidification techniques offer many advantages over conventional processing. Since rapid solidification (RS) requires high cooling rates, it can only be achieved with material that is small in at least one dimension. High cooling rates give rise to undercoolings of $100^{\circ}C$ or more before solidification, allowing large deviations from equilibrium to occur. Novel microstructures formed via rapid solidification processes are consequently observed.

The advantages gained by using a rapid solidification processing technique can be summarized as follows (see reviews 10-12):

- Microstructural refinement: Melt quenched alloys usually have finer grain size, smaller particles size, and less macrosegregation, which is a major problem found in conventionally-cast alloys. These effects increase with increasing cooling rate.
- Extension of the solid solubility limit: Larger amounts of supersaturation of solute elements have been detected as a result of RS. This can permit larger addition of alloying elements, leading to the possibility of precipitation of a significant additional volume fraction of second phase(s).
- Formation of metastable phases.
- Increased tolerance for impurity elements.

2.1.2 Production of Rapidly Solidified Material

Rapidly solidified (RS) material suitable for subsequent compaction to a solid article is made in a variety of ways such as atomization, splat cooling and melt spinning (see reviews 10,11,13). At present, atomization is the most common way of producing RS aluminum alloys in commercial quantities. Molten metal is sprayed through a nozzle and quenched by a rapidly moving gas stream. The molten droplets solidify at typical cooling rates of 10^4 to 10^6 °C/s.

Splat quenching and melt spinning can produce experimental amounts of material and are thought to provide a higher cooling rate than atomization (10^8 °C/s). In splat cooling, molten droplets are quenched on a highly conductive chilled surface. The flakes commonly produced are 2 to 3 cm in diameter and about 40 μ m thick. In melt spinning, the molten metal is brought into contact with a rapidly rotating highly conductive wheel, producing ribbon material.

During processing, an oxide layer forms on the RS particles, flakes and ribbons as a result of reaction in the melt prior to RS process or by scavenging of oxygen by the powders during handling and packaging (14). The reaction of this freshly formed oxide with humid air gives rise to a hydrated oxide layer. RS aluminum alloy particles therefore exhibit a hydrous oxide layer composed of a film of aluminum oxides and aluminum hydroxides, small amount of MgO crystallites, and the physically adsorbed gases H_2O and O_2 (15-17). This oxide layer is incorporated into the alloy during subsequent processing to a final article. It is an obstacle to the bonding process between the individual particles during compaction and leads to poor mechanical properties when incompletely broken up or non uniformly distributed during consolidation and extrusion.

To avoid the deleterious effects of incorporating hydrogen into the consolidated alloy, vacuum degassing of the particles before consolidation appears to be a general processing requirement. The quality of this degassing treatment step will determine how easily the oxide film is broken up during hot pressing and will strongly influence the effect of the oxide on final mechanical properties.

2.1.3 Consolidation of the RS particles

Figure 1 shows the most commonly used procedure for the consolidation of RS particles into a fully dense final product (cited in 10,12,15,16,18). A schematic of the oxide particle morphology corresponding to the different processing steps is shown (from 15). The different stages of consolidation are:

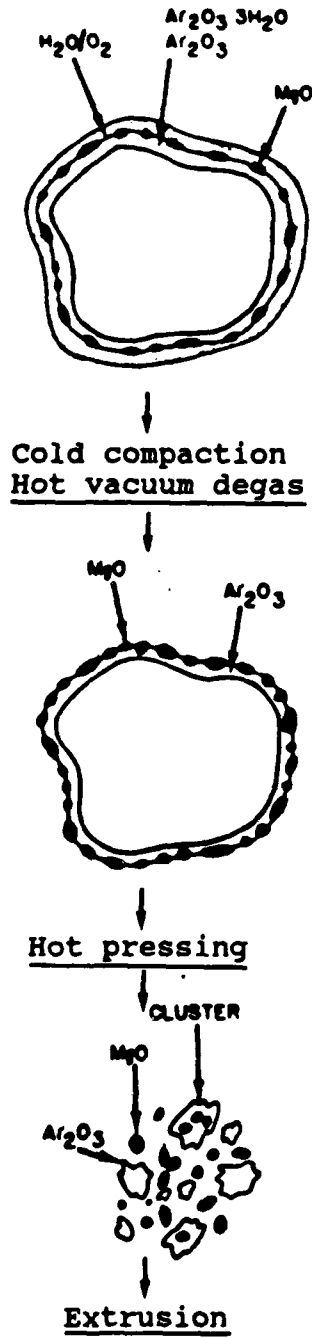


Fig. 1 Consolidation procedure for RS particles, schematic of the alloy particle oxide. (After Kim, Griffith and Froes)

-1- Cold compaction: The particles are cold compacted using pressures high enough to produce a billet that is approximately 75% theoretical density. Cold compact density is an important consideration for effective degassing which requires interconnected pores in the compacts.

-2- Hot vacuum degas: The billets are then sealed in aluminum cans to provide a means for hot vacuum degassing. During degassing, the hydroxides decompose to aluminum oxide (Al_2O_3) and H_2O , which reacts with Al and Mg atoms and forms additional Al_2O_3 and crystalline MgO. Degassing dries the "wet" surfaces of the oxide layer and increases the amount of MgO crystallites embedded in the amorphous Al_2O_3 . The combined effects arising from a proper degassing make the oxide film more susceptible to break-up by subsequent hot pressing. Failure to accomplish this step results in poor bonding between the particles, as well as porosity and blistering in the final product if the hydrogen is released from the oxide after the hot pressing process.

In rapidly solidified alloys with metastable microstructures, choosing the degassing temperature is a compromise between the need of an effective degassing and the desire to avoid coarsening of the original refined structure at excessively high temperature. Thus, the degassing treatment requires a compromise between the counterposed requirements of degassing and maintaining a fine microstructure.

-3- Hot pressing: Hot pressing fully densifies the degassed compact. The overall deformation is moderate but can be sufficient to destroy the continuity of the oxide film and break it up into Al_2O_3 film fragments, Al_2O_3 -MgO clusters and MgO crystallites.

-4- Extrusion: during hot working such as extrusion, further break-up of relatively large Al_2O_3 fragments and Al_2O_3 -MgO clusters takes place due to elongation of the original powder particles. Optimum redistribution of oxide fragments occurs over a certain range of processing parameters (temperature, pressure, ram speed, extrusion ratio). Theoretical observations made by Sheppard et al. showed that the pressure required for the extrusion of powder compacts is lower than that required for a comparable cast alloy (19). This was illustrated by comparing the extrusion pressure as a function of the extrusion rate for conventionally-cast and powder materials (19). Comparison of the pressure-ram displacement traces for three Al-Mg alloys also showed that a far lower pressure was needed to extrude a powder Al-10Mg alloy than was needed for the cast Al-7Mg and Al-5Mg alloys (20).

The potential range of processing conditions over which an alloy can be worked is illustrated on the diagram in Figure 2. The lower temperature limit is the lowest temperature at which the rate of relaxation is rapid enough to eliminate strain hardening during hot working and is determined by pressure

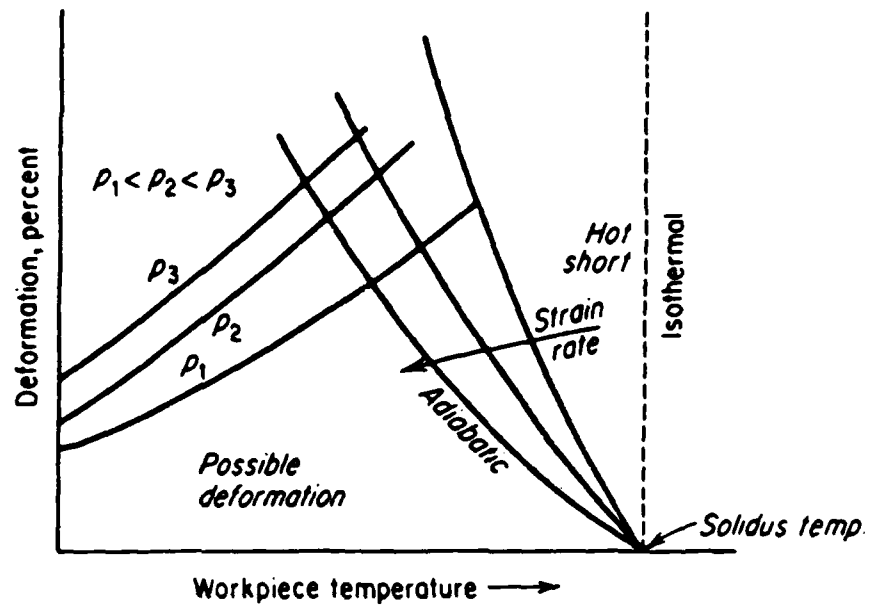


Fig. 2 Schematic effect of temperature, pressure and strain rate on the allowable working range. (After Dieter)

limitations on the extrusion press. The upper temperature limit is determined by the temperature at which melting or melting of a small amount of segregated phase (equilibrium or nonequilibrium eutectic melting) occurs, or by the temperature above which billet surface tearing takes place. The extrusion temperature, once chosen within the working window, should be low enough to prevent coarsening of the structure and to promote a fine subgrain or grain structure. Yet, higher temperatures lower the extrusion pressure, thus reducing the chance of failure during extrusion. Similarly, the extrusion ratio is a compromise between the requirements for efficient break up of the oxide film on the powder particles (higher ratio desirable) and billet size.

2.1.4 Application of RS Processing to Al-Li alloys

RS techniques have been applied to Al-Li-base alloys in an effort to overcome ductility and toughness problems that have been experienced with conventionally-cast ingots. The conventional interpretation of the low ductility and fracture toughness of ingot metallurgy processed (IMP) Al-Li-base alloys has emphasized dislocation shearing of the ordered Al_3Li precipitates which results in a high degree of planar slip during plastic deformation. One method which has been proven effective ameliorating the ductility problem associated with Al_3Li precipitates is grain size reduction, which can be achieved by applying a process involving RS. Localization of slip can also be inhibited by a high volume fraction of very fine non-shearable dispersoid particles or composite precipitates which can be obtained by the use of RS approach. The dispersoid-forming elements exhibit extended solid solubility during RS and can be subsequently precipitated uniformly as fine particles during an hot degassing or other annealing treatments.

Al-Li alloys processed by ingot technique generally contain coarse constituent particles that can act as sites for crack initiation and may contribute to poor corrosion resistance. RS promotes greater microstructural homogeneity and greater solid solubility than conventional casting methods, and therefore leads to less segregation of impurities and solute elements. The problem of macrosegregation and microsegregation encountered in ingot casting has limited the maximum Li content to 3 wt% although up to 4 wt% could be taken in solid solution (from 21,22). Further Li additions, and thereby density reduction, can be achieved by preparing the Al-Li alloys by RS.

2.2 Development of (Sub)grain Structure During Extrusion

2.2.1 Relaxation Processes

During hot working processes such as extrusion, dislocations produced by deformation are eliminated by relaxation processes

that occur during deformation and thus the relaxation processes are called dynamic. Working is often carried-out under conditions of temperature and strain rate such that these dynamic relaxation processes operate continuously right up to the die exit, ensuring the absence of work hardening in the extruded product. In the case of some alloys, processing conditions may be exploited to obtain a desired degree of work hardening, rather than achieving it with a separate deformation processing step. The relaxation processes which enable plastic flow during hot working are recovery and recrystallization.

Dynamic recovery is commonly the softening mechanism of high-stacking fault energy metals, such as aluminum and aluminum-base alloys. It is the basic mechanism that leads to the annihilation of pairs of dislocations during straining. The low dislocation density accumulated during deformation is due to the ease of cross-slip, climb and dislocation unpinning at nodes. This deformation mechanism results in the formation of a well-developed subgrain structure.

2.2.2 Influence of Microstructure on Relaxation During Extrusion

The substructure formed by dynamic recovery during extrusion of an Al-3.5Mn-0.75Al₂O₃ powder alloy was stabilized by large primary precipitates already present in the as-solidified powder material (19). The presence of these primary precipitates at subgrain boundaries in the as-extruded material provided evidence that the precipitates acted as obstacles to dislocation motion and pinned the subgrains formed during extrusion.

Sheppard et al. reported that the operative softening mechanism during extrusion of RS Al-Mg based alloy was uniquely dynamic recrystallization, contrary to most aluminum alloys which relax by dynamic recovery or by both dynamic recovery and dynamic recrystallization. A secondary phase was precipitated during extrusion of RS Al-(7,12,15)Mg-0.8Mn-0.1Cr powder alloys that was attributed to the addition of Mn and Cr (23). This fine dispersion of precipitates pinned the grain boundaries and prevented their rapid migration. Thus, the precipitates were responsible for stabilization of the dynamically recrystallized grain structure.

Variations in the as-extruded structure can also arise from alloying elements in solid solution. It was observed that the size of dynamically recrystallized grains of RSP Al-Mg alloys decreases with increasing magnesium content, regardless of the processing conditions (23). Several explanations were advanced such as the dependence of the particulate size on the magnesium content. The structure variation was finally proven to be due to the effect of magnesium solute atoms on the mode of relaxation, dynamic recrystallization in this case. Solute atoms hinder dislocation mobility and dislocation climb or cross-slip and hence facilitate the formation of dislocation tangles which will

eventually lead to a greater number of potential grain boundary nucleation sites.

In addition, the as-extruded structure can be influenced by the powder particulate size since this controls the amount of oxide incorporated into the consolidated material. In the case of RSP Al-(7,12,13)Mg-0.8Mn-0.1Cr of low oxide content, no correlation was found between the prior powder particle size and the microstructure generated by dynamic recrystallization in the extruded material (23). Thus the powder identity was totally obliterated by the recrystallization process. In contrast, the higher oxide content of RSP Al-10Mg-0.4Zr was present in the form of stringers which were aligned in the extrusion direction and which acted as effective obstacles to boundary migration (19,20). The larger grain size were associated with wider stringer spacing. The high angle boundary first formed adjacent to the oxide and migrated within the original powder particles.

2.2.3 Influence of Processing Conditions

The structure of an extrudate material is dependent upon extrusion parameters of which the most important are temperature and strain rate. Since boundaries between grains or subgrains act as obstacles to dislocation motion, finer (sub)grain sizes lead to improved mechanical strength in the extruded product. Thus the structure and strength can be controlled by variation of the processing parameters. A useful parameter representing the combined effects of strain rate and temperature is the temperature-compensated strain rate (Zener-Holloman parameter) defined as:

$$Z = \dot{\epsilon} \exp(+ \Delta H/RT)$$

where: $\dot{\epsilon}$ = mean strain rate
 ΔH = activation energy of deformation
 RT = gas constant x deformation temperature

A linear relationship was recorded between $\ln(Z)$ and the inverse of the dynamically recrystallized grain size of the as-extruded RSP Al-Mg alloys (19,20,23). A linear relationship was also observed between $\ln(Z)$ and the yield strength of the extruded material. The fact that the strength was independent of the extrusion ratio (strain) indicated, according to the authors, that the softening mechanism was either dynamic recovery or dynamic recrystallization but not a mixed deformation mode.

Little variation was found on hardness readings across the transverse section of a RSP Al-10Li-0.4Zr extrudate bar (20). This important observation indicated that there was no continuous change in structure from center to periphery as is often observed in extruded materials. The unusual structural homogeneity was attributed to the lower heat generated during powder compact extrusion.

2.3 Structure and Properties of RSP Al-Li alloys

2.3.1 Grain Structure

The microstructure of the RS particles commonly consists of a fine dendritic or a fine cellular structure depending on the alloy and solidification rate. The highest cooling rate and the smallest particle size give rise to the finest cellular structure (24,25). The degree of refinement of the microstructure of the RS particles is of primary importance for the microstructure of the extruded material.

Many of the RSP alloys described in the literature have a small amount of Zr added to prevent recrystallization during consolidation and promote formation of a fine unrecrystallized structure. The zirconium forms Al_3Zr dispersoids which pin subgrain boundaries. This effect has been extensively described in the case of conventionally-processed alloys. The microstructures of these alloys exhibit unrecrystallized grains elongated in the extrusion direction and a well-defined, fully-recovered subgrain structure (14,21,22,26). A more equiaxed microstructure in which high-angle boundaries predominate can be produced by solutionizing at high temperature, allowing more subgrain boundary motion. This occurs with only minor changes in grain size and orientation (14).

The addition of Co to a non-Zr containing alloy has been found ineffective in preventing recrystallization of a roller-quenched Al-3Li-0.2Co, despite the presence of incoherent dispersoids thought to be Al_9Co_2 (27). The recrystallized microstructure consisted of a well-defined substructure which resulted from the high temperature and high strain rate deformation that occurs during extrusion. This agrees with the results of previous investigations on Co containing IMP alloys.

In alloys produced by ingot techniques, large constituent particles are not effective in retarding recrystallization and grain growth. In the case of RSP alloys, the small size of the constituent particles can render them equally as effective as the dispersoids (in 21,28). This was the case for a splat-quenched Al-3Li-3Cu-1Mg alloy (29). The incoherent oxide particles were reported to be weak substructure stabilizers (26).

2.3.2 Oxide Particles

It has been noted previously that RS Al-Li particles are always contaminated with oxides. The oxide characteristics have been studied by several investigators (10,15,17,18). In the extruded material, the oxide is always present along the prior particle boundaries and appears as a fine dispersion of particles, as a thick continuous layer, or as discrete clumps containing several particles (respectively 22,26,28). Layers or

large groups of oxide particles can serve as easy fracture propagation paths, thereby reducing ductility and toughness. This was observed in an RSP Al-4Li alloy where large concentrations of oxides were mechanically-fibered, leading to degradation of the mechanical properties (14).

2.3.3 Constituent Particles

Meschter et al. have compared the microstructures of three RSP Al-(3-4-5)Li extrusions in their solution treated condition and found that the constituent particle density increased with the amount of Li added (14,26). Based on this observation, they concluded that these particles were Al-Li oxides which had been hydrolyzed upon exposure to ambient water vapor. These constituent particles were relatively inhomogeneously distributed in the matrix, thus it is believed that the oxides were formed by a reaction of the melt with the atmosphere and were subsequently atomized into discrete particles which were then incorporated into the extrusion.

Composition/solution treatment combinations which do not dissolve all the alloying elements leave constituent particles in equilibrium with the matrix phase. This is observed in some of the RSP Al-Li alloys (14,21,22,24,26,28). The use of RS particulates can eliminate formation of those constituents or produce significantly finer constituents than in ingot cast alloys of similar composition. A comparison of powder metallurgy processed (PMP) versus IMP Al-3Li-1.3Mn alloys revealed that both materials contained Mn-rich constituent particles with diameters less than 1 μm , but that only the IMP alloy showed the presence of much larger 10 μm Mn-rich particles (28). The small particles are thought to have formed during consolidation or mechanical processing while the large ones were formed during solidification.

Some of the RSP Al-(3-4-5)Li-0.2Zr alloys containing Mg or Cu exhibit constituent particles whose volume fraction varies with the composition and the solution heat treatment conditions (14,24,26). The conclusion is that even though these constituent particles are much finer as a result of RS approach than they would have been in an ingot cast alloy of the same composition, only 5 volume percent of these brittle particles can be tolerated with retention of acceptable ductility and toughness. For this reason, powder source Al-4Li alloys cannot incorporate a (Cu+Mg) concentration greater than 1 wt%. Formation of the AlLi phase is also a major barrier to production of Al-5Li alloys with acceptable mechanical properties and corrosion resistance (14,26).

2.3.4 RSP Al-Li Alloys Incorporating Dispersoid-Forming Elements

When elements with limited solubility in aluminum are added to Al-Li alloys, they produce intermetallic compounds at the homogenization temperature. These phases usually do not incorporate Li and, as such, do not alter the precipitation sequence. Dispersoid-forming elements commonly found in conventionally-cast Al-Li alloys include Zr used to inhibit recrystallization, Mn which controls the grain size of recrystallized products, and other elements such as iron or silicon which enter the melt as impurities to form Al-rich intermetallic particles. Iron- or silicon-rich particles are invariably deleterious to mechanical properties of conventionally-processed aluminum alloys as a consequence of their coarse size and distribution.

RSP increases the solid solubility of potential dispersoid-forming elements in Al-Li alloys by allowing a larger volume fraction of finer dispersoids to be produced than is the case for conventional processing. Commonly, these elements are in solid solution in the RS material and can subsequently be precipitated as fine dispersoids during further processing (21,22,29). In addition, RS can be exploited to incorporate other dispersoids in Al-Li matrices. Limited studies have been carried out on Al-Li based alloys containing Ti, Co, Y, Fe, Ni, Mn, V, Nb, Mo, W, and Cr in addition to Zr (24,28,29,30). The resulting dispersoids are often taken to be the corresponding Al-X intermetallic with or without Li incorporation. However, unidentified phases have been found for example in the complex microstructure of an Al-4Li-0.5Mo (30).

RS of Al-3Li-0.16Ti and Al-3Li-0.23Co alloys resulted for the first alloy in complete solution of Ti and for the second one in the formation of a fine distribution of Co containing dispersoids (29). In contrast with RS method which promoted microstructural homogeneity and greater solubility, the slow cooling rates during ingot casting of the Ti-containing alloy resulted in an extensive separation of the solute elements and the formation of coarse intermetallic segregation compounds. During consolidation and extrusion of the RS particles, some second phase precipitation did occur in the Ti-containing alloy, while the Co-containing dispersoids remained fine. Coarse heterogeneous precipitation of AlLi phase and formation of precipitate free zone (PFZ) in the vicinity of the dispersoids and grain boundary was not observed. The possible substitution of Li for Ti or Co in the dispersoids was mentioned.

Many investigations have been made on RSP Al-Li alloys containing zirconium as the dispersoid-forming element. A large volume fraction of uniformly-dispersed Al_3Zr or $Al_3(Li,Zr)$ composite precipitates is produced as a result of RS technique. It is believed that these large particles substantially influence the deformation behavior due to their non-shearable nature and are therefore desirable for the improvement of ductility and

toughness.

Allied-Signal's RSP Al-Li-Zr alloys containing Cu and Mg were given a double aging treatment for the purpose of promoting the development of composite precipitates (21). Zirconium was present in solid solution in the as-solution treated alloys and precipitated during the double aging-treatment leading to an homogeneous distribution of composite precipitates and preferential nucleation and growth of Al_3Li precipitates around the core precipitates. In the case of this study, composite precipitates did not form as a result of heterogeneous precipitation of Al_3Li upon pre-existing Al_3Zr dispersoids.

More often, a large volume fraction of Al_3Zr dispersoids is already present in the as-solutionized extruded bar (22,31). The subsequent aging treatment promotes precipitation of Al_3Li both homogeneously and on the Al_3Zr particles to give the composite $\text{Al}_3(\text{Li,Zr})$ phase. The microstructure contains homogeneously distributed composite precipitates and Al_3Li present in the matrix but mostly associated with the composite precipitates.

2.3.5 RSP Al-Li Alloys Incorporating Precipitate-Forming Elements

The use of additional precipitate-forming elements in conventionally-cast Al-Li alloys has been the subject of many investigations. The resulting precipitates affect the intrinsic slip characteristics of the matrix whereas the dispersoid-forming elements such as Zr often influence only the grain structure. Most of the research devoted to alloys of this type has concentrated on additions of Cu and Mg either separately or in combination. Within the Al-Li-Mg system, the only phases in addition to Al_3Li and AlLi are Al_3Mg_2 , $\text{Al}_{12}\text{Mg}_{17}$, and Al_2LiMg . Mg has a high solid solubility in Al which is relatively unaffected by the presence of Li. As a consequence, Mg remains in solid solution in practical alloy compositions and only heterogeneous nucleation of Al_2LiMg occurs. The precipitation sequence in Al-Li-Cu is as follows:

Solid Solution \rightarrow GP zones \rightarrow θ'' \rightarrow θ' \rightarrow (Al_2Cu) \rightarrow $T_1(\text{Al}_2\text{CuLi})$

The precipitate phases reported in quaternary Al-Li-Cu-Mg are Al_3Li , Al_2CuMg and Al_2CuLi phases.

The microstructure of precipitation-hardening alloys resulting from RS techniques generally contains the common phases of conventional casting, but is much finer. In addition, the possibility of increasing solid solubility through high cooling rate offers the potential of retaining a larger quantity of alloying elements in solid solution. The effects of additions of Cu and Mg on the microstructure of RSP Al-Li alloys containing 3, 4, 5 wt% of Li and the structure-refining element Zr was determined at McDonnell Douglas research laboratories. The RSP

Al-3Li based alloys contain a large volume fraction of Al_3Li , Al_2CuLi plates nucleated on grain boundaries for the Cu containing alloys, and precipitate free zones. The RSP Al-(4-5)Li extruded bar could be successfully produced using conventional powder consolidation methods despite the high Li level. The Al-5Li based alloys, the Al-4Li-2Cu-0.2Zr alloy and the Al-4Li-2Mg-0.2Zr alloy have more than 10 volume percent of brittle constituent particles and their microstructure was not further studied. The only phase present in the Al-4Li-1Cu-0.2Zr and Al-4Li-1Mg-0.2Zr alloys is Al_3Li in addition to a few constituent phases.

2.3.6 Mechanical Properties: Influence of Processing Conditions and Oxide Particles

Much of the data on the mechanical properties of RSP Al-Li alloys reported in the literature has clearly been influenced by processing-related problems such as incomplete bonding of particulates resulting from the presence of oxides and from failure to consolidate the RS particles efficiently (22,24,28). Typical features commonly found on the fracture surfaces of alloys with poor mechanical properties include significant amounts of delamination resulting from separation along prior particle surfaces or cracking along the prior particle boundaries due to the thick oxide layer still present in the extruded material.

The presence of oxide along prior particle boundaries render the mechanical properties very sensitive to test direction. As an example, a study made on two Al-Li based alloys of different lithium levels (3 and 3.4 wt%) showed that both alloys had similar T-L fracture toughness values, which were smaller than the two different values corresponding to the L-T orientation (22). It was suggested that the dominant factor controlling the T-L fracture mechanisms of this alloy was the oxide particles. This is consistent with the improvement in toughness resulting from an increase in powder particle size and therefore a reduced prior particle boundary area.

Palmer et al. have evaluated the effect of various processing methods on the properties of Al-3Li extruded materials whose fracture behavior appeared to be dominated by the oxide particles on prior particle boundaries (24). The mechanical properties of the investigated materials were not improved by either selective screening of the splat lots to remove most of the non-splat particulate, or increasing the extrusion ratio which, however, resulted in less delamination. A small improvement in ductility resulted from the use of multiaxial forging prior to extrusion and was attributed to better break-up of oxide films on prior particle boundaries.

The fact that the fracture behavior of RSP alloys is often dominated by oxide particles or an oxide layer on prior particle

boundaries implies that very little work has been performed to evaluate the specific effects of alloying elements such as Mg, Cu, Mn, Zr on the mechanical properties. The effect of microstructural characteristics such as dispersoid particles, grain size etc. could not be adequately assessed in many studies due to premature failure induced by oxide. For example, the elongation to failure value of a PMP Al-3Li-Mn alloy was found independent of the age hardening condition, contrary to the equivalent IMP alloy, due to the crack nucleation process dominated by large oxide particles. The potential beneficial effects of RS technique for processing can only be fully realized by improvements in melting, particulate-making and particulate processing techniques so that the oxide is minimized and well distributed. This has been done successfully by Meschter et al. on vacuum atomized and consolidated Al(3,4,5)Li based alloys.

2.3.7 Mechanical Properties: Influence of Composite Precipitates or Dispersoids

The presence of large volume fractions of homogeneously distributed composite precipitates or dispersoids found in RSP Al-Li alloys containing dispersoid elements significantly affects the deformation behavior of these alloys and, consequently, their mechanical properties. Typically, plastic deformation of Al₃Li strengthened Al-Li alloys results in severe planar slip because the Al₃Li is sheared by moving dislocations. It is one cause of the low ductility and toughness observed in these alloys. In contrast RSP Al-Li alloys containing non-shearable dispersoids or composite precipitates exhibit a more homogeneous mode of deformation due to the shear resistant nature of those particles (21,27). Dislocation loops accumulate at each of the particles by the Orowan mechanism and thus harden the active slip planes, causing transfer of slip to adjacent planes (21,27). The spreading of slip bands results in smaller stress concentrations at the head of the slip bands, which are further reduced by the fine grain size of the RSP alloys.

Several investigations show that good mechanical properties can be achieved in RSP alloys containing a fine dispersion of non-shearable Al₃(Li,Zr) precipitates. The ductility of roller-quenched extruded Al-3Li alloys containing Ti or Co has been found to be much higher than that of the equivalent binary Al-3Li alloy (27). The lower strength level is attributed by the authors to the possible substitution of Ti or Co by Li in the dispersoids which reduced the volume fraction of Al₃Li precipitates. Good combinations of strength/ductility have been observed on Al-3Li alloys containing Cu, Mg, and Zr by double-aging heat treatments which promoted precipitation of composite precipitate (21).

The dependence of the strength of an Al-2.5Li-0.6Zr alloy on the extrusion temperature has been attributed to the precipitation behavior of a Zr-bearing phase during extrusion (31). Precipitation of this phase probably occurred during the

higher temperature extrusions and, for extrusions performed at low temperature, a subsequent high temperature soak was required to precipitate this phase. This would explain why extrudates produced at high temperature develop their mechanical strength when aged directly, whereas extrudates produced at the lower temperatures were strongest when aged after a solution treatment. In addition, the higher extrusion temperatures gave somewhat better ductility and fracture toughness, as a result of the finer morphology exhibited when the precipitates are formed concomitant with strain.

2.3.8 Mechanical Properties: RSP Al-Li Alloys Incorporating Precipitate-Forming Elements.

2.3.8.1 Influence of Grain/Subgrain Structure and Zr Addition

The effect of Zr addition on the mechanical properties of RSP Al-Li based alloys is attributable to the subgrain refinement which effectively homogenizes slip and prevents the formation of intense planar slip (26). The result of the zirconium-refined substructure is higher yield stress and ductility as shown by comparison with RSP Al-3Li alloys not containing Zr. The fact that the yield stress of Al-3Li-2Cu-(0.2,0.5)Zr and Al-3Li-2Cu-0.5Co alloys were similar despite different average subgrain diameter was attributed to the effect of added copper, which is more important than the effect of varying the grain or subgrain diameter (26).

2.3.8.2 Influence of Mg Addition

Microstructural observations of peak-aged RSP Al-3Li-(1,2)Mg-0.2Zr showed no evidence of precipitated phases other than Al_3Li . Less than 2 wt% Mg is primarily present in solid solution in a large range of aging temperatures (26). Adding 1 wt% of the solution strengthening element Mg to Al-3Li-0.2Zr resulted in the increase of the ultimate tensile stress and yield stress with no loss in ductility, while a further addition of Mg to 2% had no additional effect on properties. Since up to 2 wt% Mg was fully dissolved after solution treatment at 530°C, the nearly equivalent longitudinal and transverse properties were unaffected by increasing the solution treatment or by stretching after solution treatment or both.

2.3.8.3 Influence of Cu Addition

The influence of added copper depends on whether it is fully taken into solid solution and subsequently precipitated, or if it is in excess of the solubility limits and included in constituent particles. The solution treatment temperature is therefore important. For a solution treatment temperature at 530°C, the addition of 1 wt% Cu to the ternary RSP Al-3Li-0.2Zr alloy resulted only in a small increase of the yield and ultimate tensile stress. Further addition of Cu up to 2 wt% resulted only

in the formation of a low density of constituent particles and had no influence on the mechanical properties (26). Raising the solution treatment temperature to take all the (Cu+Li) into solution resulted in an increase in the yield stress of the RSP Al-3Li-1Cu-0.2Zr and a much larger increase on the yield stress of the RSP AL-3Li-2Cu alloys (14).

2.3.8.4 Influence of the Amount of Li

The aging behavior of an RSP Al-Li-Zr alloy after solution treatment can be described as follows: the yield stress increases initially owing to Al_3Li nucleation and an increase in the average Al_3Li precipitate diameter. As aging continues into the overaging regime, the strength drops slightly and the ductility falls off as a result of grain boundary AlLi precipitation and PFZ formation (26).

A comparison of the mechanical properties of peak-aged Al-3Li-Zr and Al-4Li-Zr alloys shows that an increase in the Li concentration from 3 to 4 wt% left the yield and ultimate tensile stresses almost unchanged in spite of the increase in Al_3Li density, and decreased the ductility from 8 to 6% (14,26). The fact that the strength was not higher in the alloy with the higher amount of lithium was attributed to the larger average subgrain diameter in this alloy. In addition, a significant amount of lithium may be diverted to oxides in the Al-4Li-0.2Zr alloy, lowering the Li concentration available for Al_3Li formation and decreasing the strength. The Al-5Li-0.2Zr showed a low 0.8-4 % elongation and no work hardening in the peak-aged condition (26). This high Li content alloy always had 10 volume percent of constituent AlLi particles regardless of the solution treatment performed.

2.3.8.5 Influence of Constituent Particles

The presence of coarse insoluble constituent particles is less likely in a RSP alloy than in a conventionally cast alloy. Ideally, a RSP alloy compared to the equivalent IMP alloy has higher ductility and toughness as well as higher strength. However, many studies have been done on RSP alloys whose composition are such that they contain constituent particles. Alloys in which too much solute is tied up in insoluble constituents do not exhibit precipitation hardening since the solute is not available for precipitation, leading to very low strength levels. In addition, even though the constituent particles are finer as a result of RS approach than they would have been in an ingot cast alloy of the same composition, their high volume fraction can cause a low ductility and toughness.

The strength and ductility of RSP Al-(4-5)Li-0.2Zr alloys containing Cu or Mg was found acceptable only for alloy composition / solution-treatment combinations which yield less than 5 volume percent constituent particles (26). Study of RSP Al-3Li-(2-4)Cu-0.2Zr alloys shows that increasing the copper

content from 2 to 4 wt% results in a larger volume fraction of brittle Al_2CuLi constituent particles and thus a decrease in both the strength and the ductility (24). The mechanism of failure of the Al-3Li-4Cu-0.2Zr alloy was by void coalescence with the voids nucleating at the cracked particles.

2.4 Stabilization of the Al_3Li Phase

2.4.1 Structure of A_3B Compounds

It has been observed that the structure of ordered A_3B -type alloys consists of ordered layers and can be described in terms of various stacking sequences of these layers. The two basic types of close-packed layers that exist for A_3B compounds are designated as triangular (T) and rectangular (R) type and are shown in Figure 3. The atomic arrangement in the T layer can deviate from the ideal close packing if the radius ratio of the two atoms A and B becomes too large, giving rise to a Ni_3Sn -type layer. Stacking of the R-type layer forms structures that generally have tetragonal symmetry ($\text{D}_{022}, \text{D}_{023}$). Compounds made of T-type layers commonly have structures of cubic, hexagonal or rhombohedral symmetry. Stacking of the type ABAB corresponds to the purely Mg_3Cd -type hexagonal structure (D_{019}) and stacking of the type ABCABC corresponds to the purely Cu_3Au -type cubic structure (L_{12}).

Unfamiliar binary A_3B or quasi-binary $\text{A}_3\text{B-C}_3\text{B}$ compounds have been described as being built-up from the same T layers and as having a complex transition stacking sequences between the purely cubic stacking and the purely hexagonal stacking. Those compounds can be characterized by their percentage of hexagonal stacking calculated by counting in the unit cell the number of layers whose adjacent layers have the same stacking position. The A layer is designated as hexagonal in a ABA sequence but as cubic in a ABC sequence. For example, the Al_3Pu type structure (hexagonal crystal lattice) whose stacking sequence is ABACBCA has a 33.33 % hexagonal character.

2.4.2 Factors Affecting Intermetallic Crystal Structure and Stability

Studies of the structure of ordered compounds have revealed that both the formation of T or R layers and the stacking sequence of these layers can be correlated with fundamental alloying parameters such as the radius ratio of A and B atoms and the concentration of valence electrons. Identification of these factors and their connection with the known crystal structure is of primary importance for control of ordered crystal structure through macroalloying.

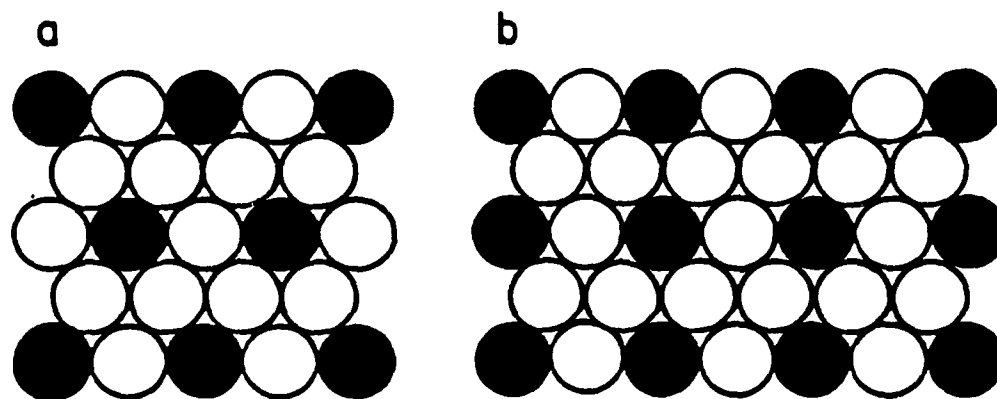


Fig. 3 Atomic structure on close-packed layers in: (a) T-type ordered structure, and (b) R-type ordered structure. (After Liu)

In their study of binary transition element A_3B alloys, Beck and Dwight correlated the crystal structure type with the valence electron / atom ratio (e/a), despite a large difference in the A and B atoms' atomic size (32,33). With an increase in e/a , the structure made of T-type layers changed from purely cubic stacking (Cu_3Au type) to purely hexagonal stacking (Mg_3Cd type) with the intermediate structure having 50 % of hexagonality character (Ni_3Ti type). Further increase in e/a led to a change in the basic layer structure from T to R type.

Investigation of several quasi-binary A_3B systems with vanadium as A-component and nickel, cobalt and iron or a mixture of these elements as B-components has been pursued by Sinha and Liu, as described by Liu (34). The stacking sequence and therefore the percentage of hexagonal character was also correlated with the e/a ratio. e/a in the Co_3V alloy was gradually increased by partial replacement of Co with Ni, leading to an increase in hexagonal character from 33.3 % to 100 % and, finally, to a change of the basic layer from T to R type in the case of Ni_3V alloy. On the other hand, e/a in Co_3V alloy was decreased by partial replacement of Fe for Co, leading to a reduction in hexagonal character from 33.3 % to 0 %. The $L1_2$ ordered cubic structure was stabilized in $(Co,Fe)_3V$ and $(Ni,Co,Fe)_3V$ alloys.

Watson rederived electronegativity scales and correlated the structure of AB , AM , AM_2 compounds to the resulting parameters (M is for a non-transition metal and A and B for transition metals) (35). The first parameter is an electronegativity difference term with the electronegativity similar to that of Pauling. The second parameter is $S(A)+S(B)$ for AB compounds or $S(A)$ for AM and AM_2 compounds, S being a measure of relative binding energy of s and p electrons and hence of their propensity to be involved in charge transfer and bonding. For each of the 3 types of compounds, the structure was indicated on the corresponding plot as a function of both parameters. Generally, compounds with particular crystal structures were grouped in different regions of the plots.

In contrast, Van Vucht and Buschow pointed out a correlation between the atomic radius ratio R_R/R_{Al} and the percent hexagonal character of the stacking of the T layers in rare-earth trialuminides (Al_3R compounds: R = rare-earth element) (36,37). The smaller the atomic radius ratio is (heavier rare-earth element), the less the T layer has a tendency to deviate from its ideal close packing, thus favoring cubic stacking of the layers. As the ratio R_R/R_{Al} gradually decreased, the stacking sequence of the T layers changed step-by-step from completely hexagonal (Mg_3Cd type structure) to completely cubic (Cu_3Au -type structure) through a mixture of hexagonal and cubic sequences of various percentage of hexagonal character. The gradual variation in the average atomic radius of the rare-earth element in the R sublattice resulted from mixing of these elements.

In addition to the above considerations, other factors affect the structure type of intermetallic alloys. Small contamination, sample preparation method, heat treatment, cooling rate, can explain the fact that different investigators may observe different crystal structures for compounds of the same stoichiometry. The case of the Al_3Y compound which has been studied by several authors is typical (37-39).

2.4.3 Application to Stabilization of Al_3Li Phase

When Al-Li alloys containing a large amount of Li are quenched rapidly enough so that formation of coarse primary phases is prevented, decomposition of the Al-Li solution only occurs by precipitation of the Al_3Li phase. Heat treatment of this material at temperatures above $350^\circ C$ leads to the formation of AlLi phase, as shown by the binary phase diagram of Figure 4 (in review 40). The AlLi formation can be avoided if the Al_3Li phase becomes the equilibrium phase at temperatures higher than $350^\circ C$ so that the equilibrium between Al and AlLi phases is replaced by an equilibrium between Al and stabilized Al_3Li phases.

The two concepts presented previously show that the structure of ordered A_3B compounds can be correlated with the radius ratio and electronegativity difference between the two atoms. If two elements occupy the A or B sublattice, the structure can often be correlated with the average character of the elements. These ideas have been applied, for example, by Sinha & Liu to control the ordered crystal structure of Co_3V macroalloyed with iron and nickel. In principle, these concepts can be used for stabilization of Al_3Li phase in its purely cubic Cu_3Au -type structure through macroalloying with a suitable third element "X" forming an $Al_3(Li,X)$ or an $(Al,X)_3Li$ compound.

A survey of binary Al_3X -type compounds shows that their crystal structure can be correlated to both the radius ratio (R_X/R_{Al}) and the electronegativity difference ($En_X - En_{Al}$). These compounds characteristics are listed in Table 1. The different crystal structures obtained are pointed out on the map of Figure 5 as a function of the electronegativity difference and of the radius ratio. The important result is that different structures occupy different regions of the plot.

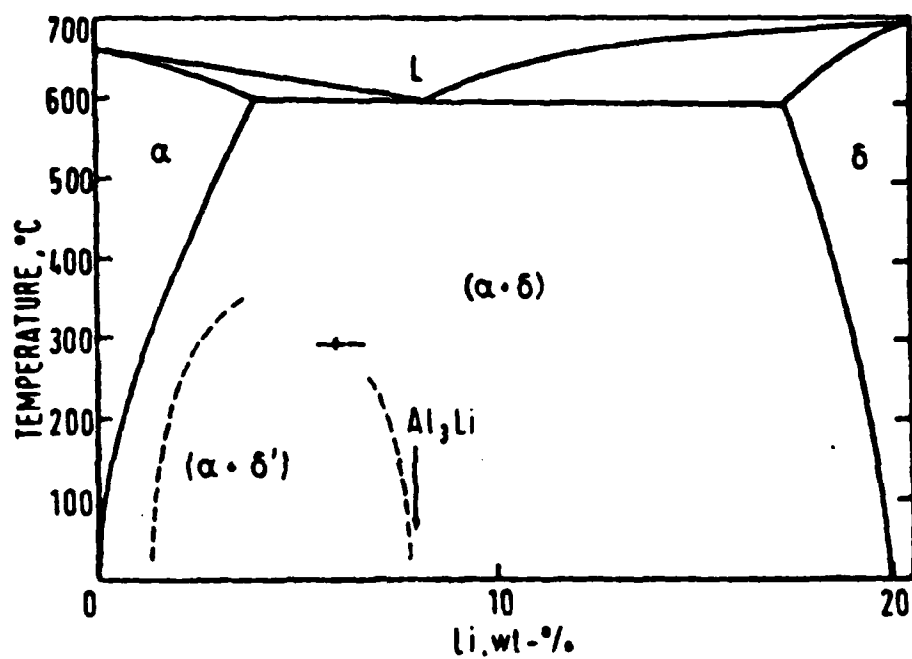


Fig. 4 Aluminum-Lithium phase diagram. Dashed lines represent metastable Al₃Li solvus. (After Flower and Gregson)

Table 1

Characteristics of Binary Al₃X Compounds

X	Alloy	Crystal Structure	R_X/R_{Al} [*]	EN_X-EN_{Al} ^{**}
Ni	Al ₃ Ni	D0 ₂₀	0.87	0.3
Fe	Al ₃ Fe	*****	0.89	0.22
Mn	Al ₃ Mn	*****	0.92	-0.06
V	Al ₃ V	D0 ₂₂	0.95	0.02
Pd	Al ₃ Pd	D0 ₂₀	0.96	0.59
Ta	Al ₃ Ta	D0 ₂₂	1.02	-0.11
Ti	Al ₃ Ti	D0 ₂₂	1.03	-0.11
Nb	Al ₃ Nb	D0 ₂₂	1.03	-0.01
U	Al ₃ U	L1 ₂	1.10	-0.23
Hf	Al ₃ Hf	D0 ₂₃	1.10	-0.31
Li ⁺⁺	Al ₃ Li	L1 ₂	1.10	-0.63
Zr	Al ₃ Zr	D0 ₂₃	1.12	-0.28
Zr ⁺⁺	Al ₃ Zr	L1 ₂	1.12	-0.28
Sc	Al ₃ Sc	L1 ₂	1.14	-0.25
Tm	Al ₃ Tm	L1 ₂	1.21	-0.36
Er	Al ₃ Er	L1 ₂	1.23	-0.37
Ho	Al ₃ Ho	(R3m)	1.23	-0.38
Yb	Al ₃ Yb	L1 ₂	1.24	-0.51
Dy	Al ₃ Dy	(R3m)	1.24	-0.39
Tb	Al ₃ Tb	(R3m)	1.25	-0.41
Th	Al ₃ Th	D0 ₁₉	1.26	-0.31
Y	Al ₃ Y	(R3m)	1.26	-0.39
Gd	Al ₃ Gd	D0 ₁₉	1.26	-0.41
Sm	Al ₃ Sm	D0 ₁₉	1.26	-0.44
Nd	Al ₃ Nd	D0 ₁₉	1.27	-0.47
Ce	Al ₃ Ce	D0 ₁₉	1.27	-0.49
Pr	Al ₃ Pr	D0 ₁₉	1.28	-0.48
La	Al ₃ La	D0 ₁₉	1.32	-0.51

* Ratio of Goldschmitt radii.

** Electronegativity (Paulings) difference.

++ Stabilized in aluminum matrix

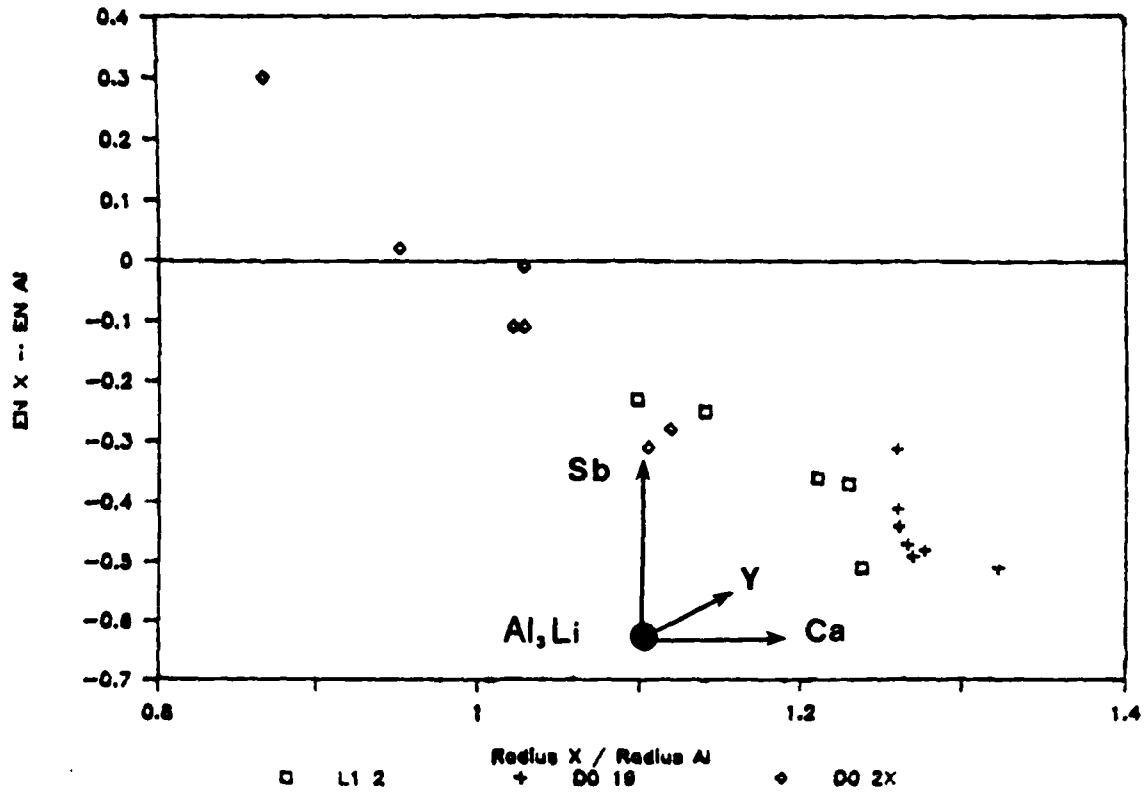


Fig. 5 Binary trialuminide compounds with structures indicated as a function of electronegativity difference and radius ratio.

One can see that the metastable Al_3Li phase lies far outside the region where other trialuminide compounds with the Ll_2 structure are grouped. The position of the Al_3Li phase on this plot can be modified by addition of an alloying element X which, by substituting partially on the Li sublattice, increases the average radius ratio or electronegativity difference or both of the $\text{Al}_3(\text{Li},\text{X})$ phase so that this phase approaches the group of compounds having the Ll_2 crystal structure. Based on this approach to the factors that establish intermetallic alloy structure and stability, it is suggested that modification of those two characters on the Al_3Li phase via an element X addition could lead to stabilization of the $\text{Al}_3(\text{Li},\text{X})$ phase in an Ll_2 crystal structure.

The anticipated effects of substitution of yttrium, antimony or calcium on the Li sublattice is shown on Figure 5. The average atomic radius ratio and electronegativity difference of the compounds $\text{Al}_3(\text{Li}_{1-x},\text{X}_x)$ have been calculated using a simple rule of mixture with x values ranging from 0 to 0.3. Addition of zirconium increases the electronegativity difference but decreases the radius ratio. On the other hand, the Al_3Zr phase in metastable equilibrium with aluminum has the same Ll_2 structure as Al_3Li , and a Ll_2 ordered $\text{Al}_3(\text{Li},\text{Zr})$ phase is thought to exist in the Al-Li-Zr system.

The Al-2.34Li-1.07Zr alloy studied by Gayle and Vandersande was produced using rapid solidification processing in an attempt to modify the Al_3Li phase to a complex $\text{Al}_3(\text{Li},\text{Zr})$ phase (41,42). Calculation of interfacial energy, chemical free energy and strain energy effects showed that homogeneous nucleation of $\text{Al}_3(\text{Li},\text{Zr})$ is favored over nucleation of Al_3Zr (41). Discontinuous and continuous precipitation of $\text{Al}_3(\text{Li},\text{Zr})$ did occur following extrusion and solution heat treatment. This phase was seen to be stable as a very fine distribution at high temperatures due to its low interfacial energy and the low solubility and diffusivity of zirconium in aluminum. An electron energy loss spectroscopy (EELS) study of the as heat-treated alloy indicated that the precipitate present at high temperature is indeed $\text{Al}_3(\text{Li}_x,\text{Zr}_{1-x})$ where x appears to be 0.45 to 0.8, which implies significant intersolubility of Al_3Li and Al_3Zr (42). The lack of strong transmission electron microscope (TEM) dark field image of the $\text{Al}_3(\text{Li},\text{Zr})$ was explained on the basis of structure factor calculation for a Ll_2 ordered Al_3Zr phase as a function of the amount of Li on the Zr sublattice (42).

The $\text{Al}_3\text{Li} / \text{Al}_3\text{Zr}$ interface, the $\text{Al}_3\text{Li} / \text{matrix}$ interface, and composition of Al_3Zr precipitates have been analyzed in an RSP Al-3.4Li-0.5Zr alloy using the techniques of high resolution electron microscopy (HREM) and image simulation (43). Agreement between experimental and calculated images of $\text{Al}_3\text{Li} / \text{Al}_3\text{Zr}$ interface suggested the probable incorporation of Li in Al_3Zr precipitates.

Considerations other than those based on the intermetallic crystal structure study have to be taken in account when the choice of a ternary element X capable of promoting stabilization of $Al_3(Li,X)$ phase of $L1_2$ -type structure is made. In the microstructure found in the alloy studied by Gayle & Vandersande, the Al_3Li phase either preferentially nucleated at the $Al_3(Li,Zr)$ / matrix interface resulting in a composite precipitate, or in some cases precipitated independently of the $Al_3(Li,Zr)$. The formation of the high Zr $Al_3(Li,Zr)$ phase occurred at much higher temperatures than that of the Al_3Li phase. In addition, the diffusivity of Zr in Al is very low compared to that of Li, thus these two elements did not interdiffuse to form a unique $Al_3(Li,Zr)$ compound. It is possible that a higher Zr level in the alloy would only result in a higher Zr concentration in the $Al_3(Li,Zr)$ phase and that the metastable Al_3Li phase would still be present at the interface and in the matrix.

2.5 Al-Li-Mg Alloy System

The aging sequence for Al-Li-Mg alloys was determined by Thompson and Noble (44) to be:

Supersaturated solid solution --> Al_3Li --> Al_2LiMg

Study of Al-(2,2.5)Li-(2,4,6)Mg alloys shows that Mg added up to 2 wt% remains in solid-solution and contributes to the strength by solid-solution hardening (44,45). The only effect of these additions was to reduce the solubility of Li, increasing the volume fraction of Al_3Li precipitates. It has been suggested that a small amount of Mg may also be incorporated in the Al_3Li phase, producing a stronger precipitate (45).

When added in larger amounts, Mg enters the precipitation sequence and is incorporated in the Al_2LiMg equilibrium phase. This phase forms as a result of overaging by heterogeneous nucleation on grain or sub-grain boundaries. Fridlyander et al. suggested that it is responsible for the good mechanical properties of the Al-Li-Mg system (46,47). The work of Thompson and Noble however showed that the coarsely dispersed Al_2LiMg precipitate which consumes the Al_3Li phase as it grows but produces little strengthening. In both their low and high Mg content alloys, the phase responsible for strengthening was Al_3Li phase, the role of Mg being one of solid-solution strengthening (44). The ternary Al_2LiMg phase precipitated at grain boundaries inhibits grain boundary deformation, reduces the strength of the boundaries, produces Al_3Li precipitate free zones adjacent to the boundaries and therefore is responsible for the brittle grain boundary failure which results in low strength, ductility and fracture toughness (45,48).

Isothermal sections of the ternary phase diagrams have been determined by different authors (46,49,50). The isotherm at 400°C determined by Levinson and McPherson is presented on Figure

6. The ternary Al_2LiMg phase has a small solubility range and is in equilibrium with the Al, Mg, AlLi, and $\text{Al}_{12}\text{Mg}_{17}$ phases. Al_2LiMg precipitates have been found in the form of rod or lath-shaped particles with $\langle 110 \rangle$ growth directions (44). It has a complex fcc crystal structure with lattice parameter 2 nm and the following orientation relationship with the matrix:

$$(-110)_{\text{ppt}} // (-110)_{\text{Al}} ; [110]_{\text{ppt}} // [111]_{\text{Al}} \text{ (no1)}.$$

when precipitated in the form of rods or laths in Al-Li-Mg alloys that can be fully solutionized.

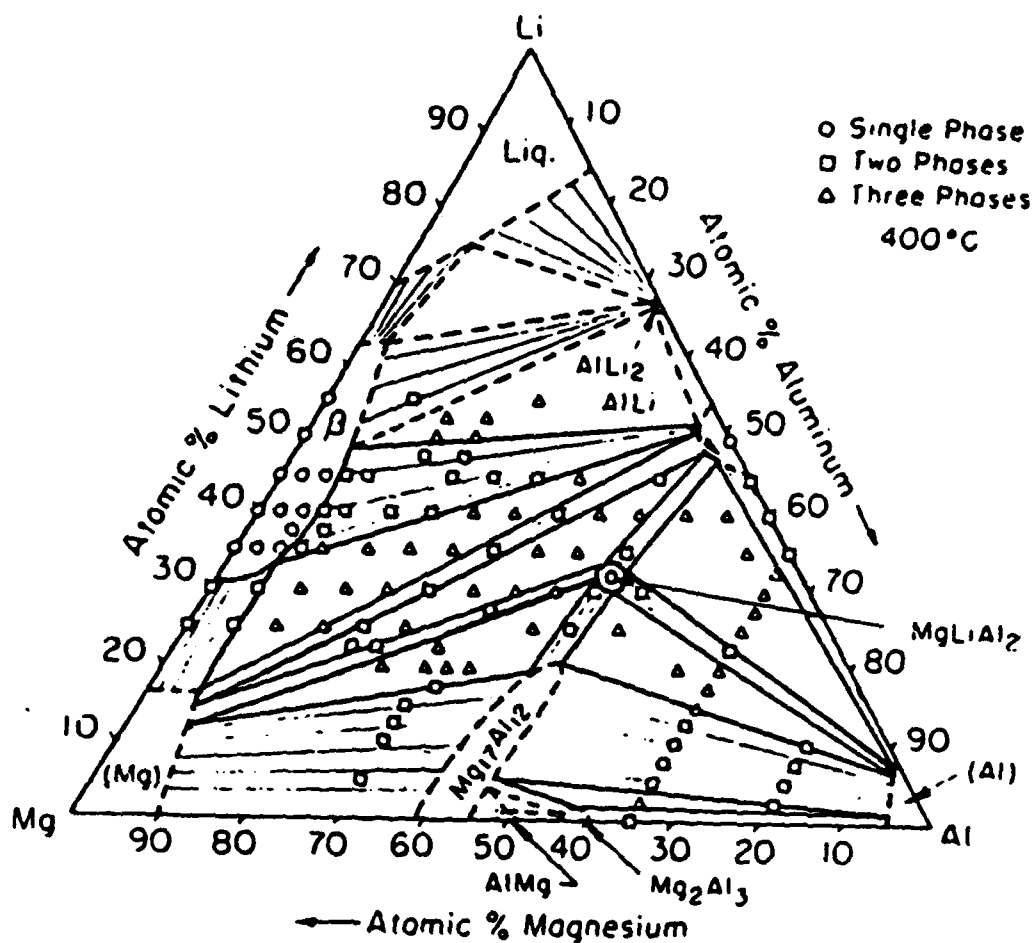


Fig. 6 Isothermal section of the Al-Li-Mg ternary phase diagram at 400°C. (After Levinson and McPherson)

3. EXPERIMENTAL PROCEDURE

3.1 Materials and Heat-Treatment

The alloys investigated in this study were prepared using rapid solidification techniques at Lockheed Palo Alto Research Laboratory. The materials examined during the first part of this study consisted of four Al-Li-Mg alloys, two Al-Li-Y alloys and two Al-Li-Sb alloys; these materials were produced by splat quenching. The nominal composition of these alloys is listed in Table 2.

Direct microstructural analysis of the flakes in the as-splat quenched condition was conducted. The microstructure and deformation properties were also studied on samples of the flakes which were annealed to simulate a consolidation process. Since heat treatment of Al-Li alloys is known to cause loss of lithium at the surface, the samples were placed in a sample holder made of a conventionally-cast Al-3wt%Li alloy to minimize the lithium depleted layer. The samples were then encapsulated in evacuated silica tubes, annealed for two hours at 300°C for the Al-Li-(Y,Sb) alloys and at 400°C for the Al-Li-Mg alloys, and cooled to room temperature. The annealed samples of the flakes exhibited a surface layer devoid of precipitates, typically 10 to 50 μm in thickness. An alloy of nominal composition Al-5Li-8.5Mg (wt%) was selected for production of a consolidated material, based on the results of the flake studies.

In the second part of this program, melt-spun ribbon of the nominal composition Al-5Li-8.5Mg (wt%) was produced. Chemical analysis made at Lockheed revealed that the actual alloy composition is Al-5.65Li-9.8Mg (wt%), considerably exceeding the nominal composition. The ribbons were cut into small flakes, cold compacted, vacuum degassed and hot pressed to 100% density at a temperature of 400°C for approximately 30 min, then extruded at 400°C into a bar with a rectangular cross section and rounded corner. Extrusion was performed with a tapered die and an extrusion ratio of 20:1. This was conducted at Lockheed Palo Alto Research Laboratory. A few flakes of the ribbon were annealed for two hours at 400°C, using the same method as for samples of splat quenched flakes. This material was examined in the as-rapidly solidified ribbon form, in the annealed ribbon form and in the as-extruded form.

3.2 Microstructural Characterization

The microstructures of the alloys were studied using the techniques of optical microscopy, transmission electron microscopy (TEM), x-ray diffraction and scanning electron microscopy (SEM). Optical metallography specimens were molded in epoxy resin, polished using standard methods, and etched with Kellers reagent unless another reagent is specified. TEM was

Table 2

Nominal Composition of Al-Li-X Alloys
(Balance Al)

X	Designation	Amount of Li		Amount of X	
		Wt%	At%	Wt%	At%
Mg	Al4Li6.5Mg	4.0	15.0	6.5	7.0
	Al4Li8Mg	4.0	15.0	8.0	8.5
	Al5Li8.5Mg	5.0	18.0	8.5	8.8
	Al5Li10Mg	5.0	18.0	10.0	10.5
Y	Al4.6Li5.9Y	4.6	18.0	5.9	1.8
	Al4.5Li9.8Y	4.5	18.0	9.8	3.0
Sb	Al4.5Li8Sb	4.5	18.0	8.0	1.8
	Al4.4Li13Sb	4.4	18.0	13.0	3.0

performed using a Phillips 400 (120 KeV) electron microscope. Thin foils were electropolished using a double jet polishing apparatus and an electrolyte consisting of Methanol and Nitric acid solution (3:1) ratio, at a temperature of -35°C and a voltage of 15 volts. Energy Dispersive Spectroscopy (EDS) was used to detect the presence of the alloying elements, except Li which cannot be detected by this method.

X-ray diffraction was performed to identify the second phases, using the pinhole method with the film-sample distance of 30 cm, a typical exposure time of 3 hours, and a $\text{Cu K}\alpha_1$ radiation. The SEM (Jeol model 35) in conjunction with an energy dispersive x-ray analyzer (EDAX) was used to identify the elements present in large constituent second phases, except Li. The fracture surfaces of broken samples of the flakes were observed with the SEM.

3.3 Property Characterization

The density of the alloys was measured using a technique based upon Archimedes' principle. Samples were weighed with a Metler electronic balance both in air and, suspended from a thin copper wire, in pure ethanol. The density of the pure ethanol was corrected according to its temperature. Alloy density, ρ , was calculated using the following equation:

NADC 88078-60

$$\rho = W_A * \rho_E / (W_A - W_L)$$

with: W_A = weight of sample in air
 W_L = weight of sample in ethanol adjusted for the wire
 ρ_E = density of ethanol

Microhardness measurements were performed using a Kentron microhardness tester, and a diamond pyramid indenter. The diamond pyramid hardness number (DPH) is expressed by the following formula:

$$DPH. = 2 * L * \sin(\alpha/2) / D^2$$

with L: Applied load (Kg)

$\alpha = 136^\circ$ = angle between opposite faces of diamond
D = average length of the indentation diagonals (mm)

The tests were conducted on the optical samples using loads of approximately 0.3 kg for the flakes and 1 kg for the extruded bar.

4. EXPERIMENTAL RESULTS

4.1 Characterization of the Materials

The as-received splat quenched flakes had diameters varying from 35 to 60 mm for the Al-Li-Mg alloys and 20 to 25 mm for the Al-Li-(Y,Sb) alloys. Their thicknesses ranged from 0.4 to 0.8 mm for the Mg containing alloys and from 0.2 to 0.4 mm for the other set of alloys, except for the flake Al₄Li₈Mg whose thickness was only 0.1 mm.

The melt spun ribbon material had the following typical dimensions: width of 2 mm, thickness of 50 to 100 μm , length of 3 to 7 cm. The discontinuous nature of the ribbon probably resulted from precipitation of a large volume fraction of Al₃Li during cooling which made it brittle. The extruded bar exhibited edge cracking along most of the length, although a region in the center of the bar was sound and could be used for preparation of specimens of various types. Dimensions of the extruded bar were 13 mm in the long transverse direction and 6 mm in the short transverse dimension.

Two values for density are listed in Table 3: the estimated values were calculated by assuming that all of the alloying elements were in solid solution and using the atomic weights of the alloy components, the measured values were found by Archimedes' principle.

Table 3
Alloy Density

Alloy	Density (Mg/m^3)	
	Predicted	Measured
Al ₄ Li _{6.5} Mg:	2.41	2.42
Al ₄ Li ₈ Mg:	2.40	2.55
Al ₅ Li _{8.5} Mg:	2.34	2.39
Al ₅ Li ₁₀ Mg:	2.34	2.22
Al _{4.6} Li _{5.9} Y:	2.47	2.41
Al _{4.5} Li _{9.8} Y:	2.54	2.44
Al _{4.5} Li ₈ Sb:	2.53	2.37
Al _{4.4} Li ₁₃ Sb:	2.63	2.42
Extruded bar*:	-	2.22

*: Actual composition Al-5.65Li-9.8Mg (wt%)

4.2 Study of the Al-Li-Mg Flakes

4.2.1 RS Microstructure

A fine grain structure observed in the four Al-Li-Mg alloys, shown on the TEM micrographs of Figure 7, was formed during rapid solidification. The finest structure is in flakes Al₄Li₈Mg and Al₅Li_{8.5}Mg which are the thinnest (respectively 0.1 and 0.4 mm) and which have therefore been subjected to higher solidification rates. The features visible in the optical micrographs of the flake cross-sections are believed to be an etching effect due to grain boundaries, Figure 8.

Precipitation of a fine dispersion of Al₃Li particles occurred during the rapid cooling of the four alloys. A typical dark field image of Al₃Li precipitates taken with alloy Al₄Li_{6.5}Mg is shown in Figure 9. Alloys Al₄Li_{6.5}Mg, Al₄Li₈Mg, and Al₅Li_{8.5}Mg were quenched rapidly enough to prevent formation of coarse second phase which would have occurred with the use of conventional solidification methods due to the alloy compositions exceeding the solubility limits. The rapid solidification technique is essential to retaining all the alloying elements in supersaturated solid solution or precipitated as fine Al₃Li. Only flake Al₅Li₁₀Mg contains constituent particles, as shown in Figure 7.

4.2.2 Annealed Microstructure

Optical microscopy performed on cross-sections of flake samples annealed at 400°C for 2 hours revealed the presence of large amounts of second phase in alloys Al₄Li_{6.5}Mg, Al₅Li_{8.5}Mg, and Al₅Li₁₀Mg; see Figure 10. The measured volume fractions are given in Table 4. The alloy compositions are such that the phase equilibria at 400°C should be between the Al₂LiMg phase and the Al matrix containing Li and Mg in solid solution, according to the phase diagram presented in Section 2.5 (50).

Table 4

Volume Fraction of Second Phase in Annealed Al-Li-Mg Flakes

Flake	Volume fraction of second phase
Al ₄ Li _{6.5} Mg	12 %
Al ₄ Li ₈ Mg	-
Al ₅ Li _{8.5} Mg	23 %
Al ₅ Li ₁₀ Mg	35 %



Al4Li6.5Mg



Al4Li8Mg

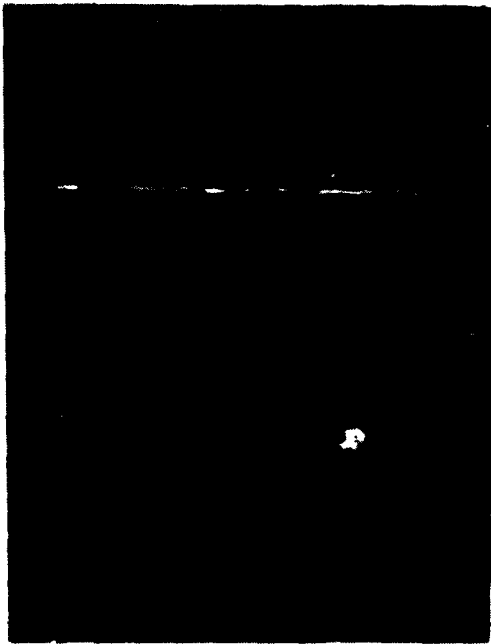


Al5Li8.5Mg

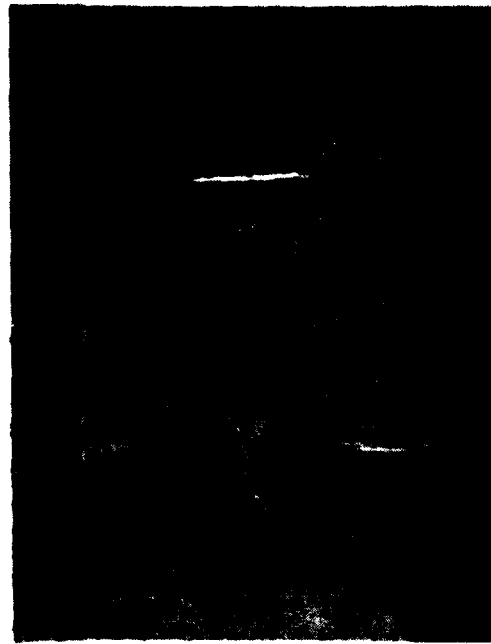


Al5Li10Mg

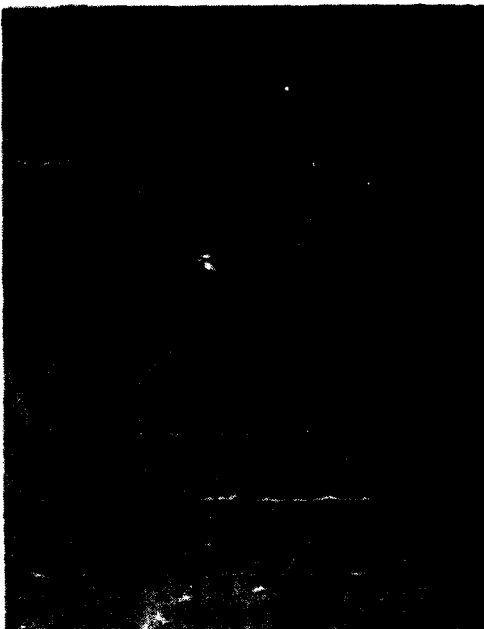
Fig. 7 TEM micrographs of as-splat quenched Al-Li-Mg flakes.



Al4Li6.5Mg



Al4Li8Mg



Al5Li8.5Mg

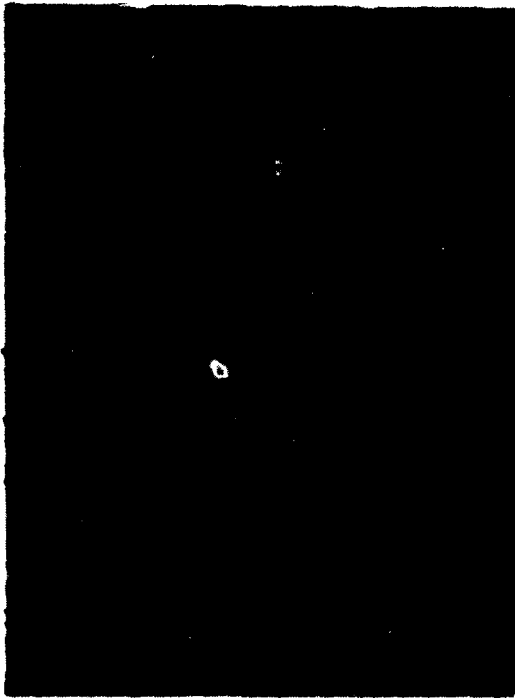


Al5Li10Mg

Fig. 8 Optical micrographs of as-splat quenched Al-Li-Mg flakes.



Fig. 9 Dark field TEM micrograph showing Al₃Li precipitates in an as-splat quenched Al-Li-Mg flake.



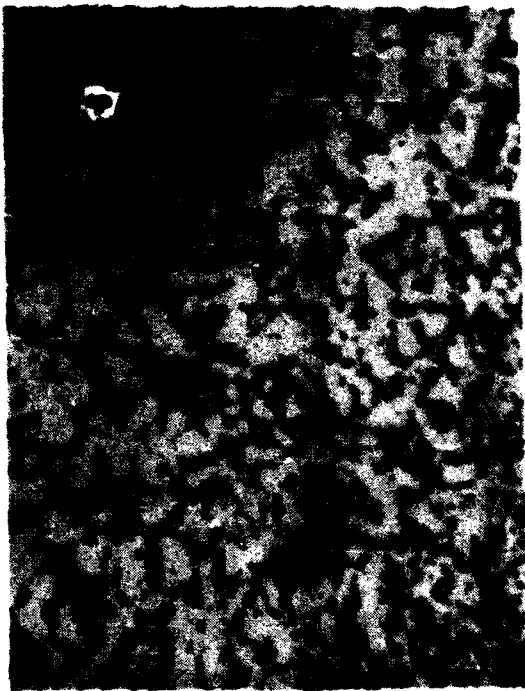
Al4Li6.5Mg



Al4Li8Mg



Al5Li8.5Mg



Al5Li10Mg

Fig. 10 Optical micrographs of annealed Al-Li-Mg flakes.

The optical samples were etched with the "Mag" reagent (20 ml conc. HF, 20 ml conc. HNO₃, 60 ml glycerol) known to stain the Al₂LiMg phase brown (50); the observed second phase stained brown indicating that it is Al₂LiMg. Furthermore, x-ray diffraction performed using the pinhole method on annealed samples of flakes Al₄Li_{6.5}Mg, Al₅Li_{8.5}Mg and Al₅Li₁₀Mg confirms the presence of Al₂LiMg phase. In addition to the two Al rings, very faint rings whose corresponding interplanar spacings match with the interplanar spacings of the Al₂LiMg phase were obtained. One can conclude that, as expected, decomposition of the Al₃Li phase and precipitation of the Al₂LiMg phase did occur during the annealing treatment at 400°C in three of the four flakes.

The case of flake Al₄Li₈Mg is different. No precipitation of a second phase during the annealing treatment was detected, as shown by the similar alloy microstructures in its as-splat quenched condition and after having been annealed for 2 hours or even 24 hours. It is believed that the actual composition of alloy Al₄Li₈Mg is below the nominal composition, which would explain why its density is greater than 2.5 Mg/m³, as well as the absence of Al₂LiMg phase after the 400°C annealing treatment.

The microstructure of annealed samples of flakes Al₄Li_{6.5}Mg and Al₄Li₈Mg was observed using the TEM and is shown on the micrographs of Figure 11. Thin foils could not be properly polished for alloy Al₅Li₁₀Mg, probably because of the high volume fraction of the Al₂LiMg phase and of the possible presence of the reactive AlLi phase. The large precipitates visible on the micrographs correspond to those previously illustrated in the optical samples and identified as the Al₂LiMg phase. No electron diffraction information could be obtained due to their thickness, but energy dispersive spectroscopy confirmed that the Mg/Al ratio was higher in the precipitates than in the matrix.

A fine dispersion of Al₃Li precipitates similar to that observed in the as-splat quenched flakes was also detected using electron diffraction. The presence of Al₃Li in the microstructure after annealing at 400°C can be explained in the following way. The phase equilibrium was established at the annealing temperature between the Al matrix containing Li and Mg in solid solution and the Al₂LiMg phase. During cooling to room temperature, part of the Li left in solid solution precipitated as the metastable Al₃Li phase.

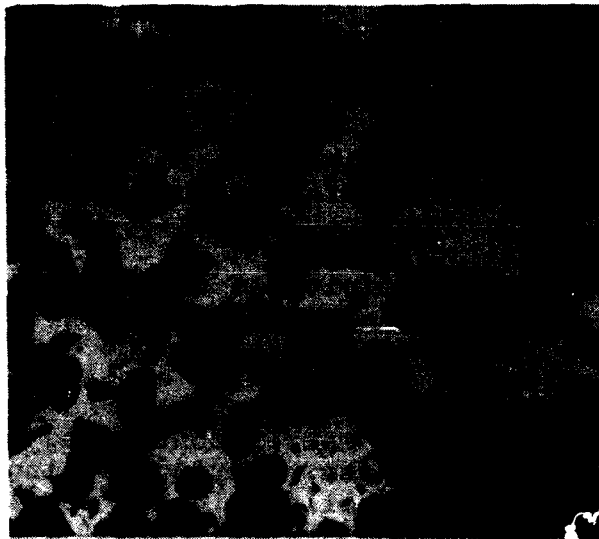
4.2.3 Deformation Characteristics of Flakes

4.2.3.1 Fracture Surface of Annealed Flakes

The fracture mode of the annealed flakes Al₄Li_{6.5}Mg, Al₅Li_{8.5}Mg and Al₅Li₁₀Mg was determined by examining the fracture surfaces of annealed flake specimens in the SEM. TEM foil sized-samples were broken manually in a manner that corresponds to a



Al4Li6.5Mg



Al5Li8.5Mg

Fig. 11 TEM micrographs of annealed Al-Li-Mg flakes.

bending-type test. Micrographs of the fracture surfaces shown on Figure 12 indicate two different of fracture modes.

Annealed flakes Al₄Li6.5Mg and Al₅Li8.5Mg fractured by coalescence of voids which probably initiate at Al₂LiMg particles. The microvoid size approximately corresponds to the interparticle spacings, which are smaller in annealed flake Al₅Li8.5Mg than in annealed flake Al₄Li6.5Mg. According to the fracture behavior of the annealed flakes, the consolidated materials of the same composition might be expected to have acceptable ductility and toughness.

Fracture of annealed flake Al₅Li10Mg appears to occur by interphase decohesion. The high volume fraction Al₂LiMg precipitate phase is distributed in a continuous network, as can be seen in Figure 10, and the precipitate-matrix interface is an easy path for propagation of cracks. Consolidation of this alloy would be expected to result in a brittle material since fracture along the continuous network of intermetallic particles would not be affected by the consolidation processing steps.

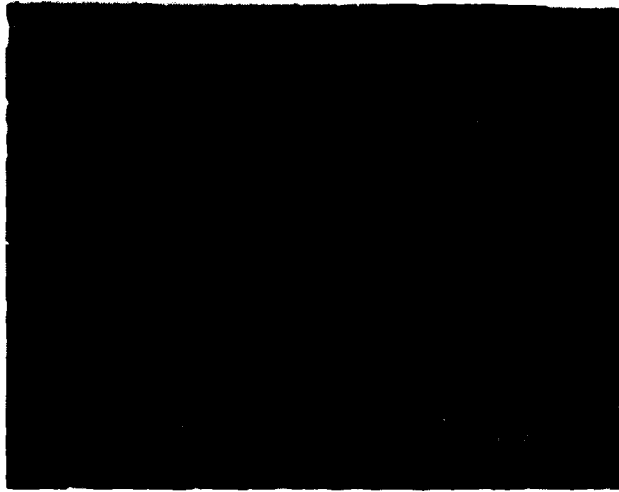
4.2.3.2 Micro-Hardness Measurements

Micro-hardness measurements were made on cross sections of as-splat quenched and annealed samples of the four flakes. The values are presented in Figure 13. Splat quenched Al₄Li6.5Mg and Al₅Li10Mg alloys show a decrease in hardness after the 2-hour annealing treatment, whereas alloys Al₄Li8Mg and Al₅Li8.5Mg need a longer heat-treatment to exhibit a hardness decrease. Some precipitation of a second phase, revealed by a slight increase of the hardness, does occur in alloy Al₄Li8Mg, despite the evidence that insufficient alloying elements are present for Al₂LiMg precipitation.

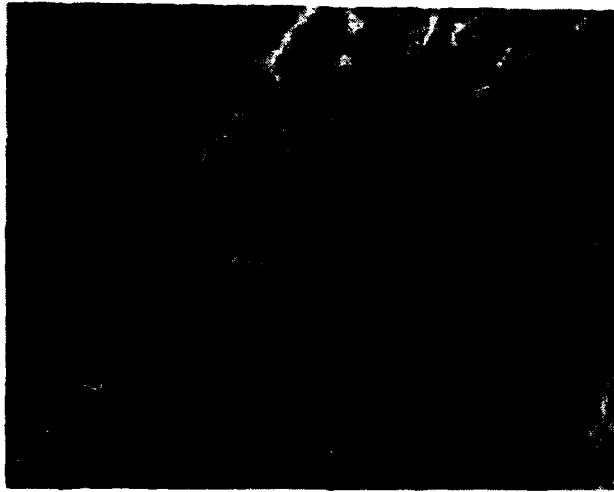
Precipitation of the Al₂LiMg phase leads to some precipitation hardening but these precipitates coarsen rapidly during annealing at 400°C, resulting in a decrease in hardness. The large particles do not provide much particle-strengthening. A large part of the drop in hardness can be attributed to a loss in solid solution strengthening. Magnesium, which is known to be a strong solid solution strengthening agent in aluminum alloys, enters the precipitation sequence during the annealing treatment to form the Al₂LiMg phase. The fraction of Mg atoms left in solid solution, as well as their contribution to alloy strength, decrease considerably during the annealing treatment.

The hardness decrease is also representative of the dissolution of the metastable Al₃Li phase at 400°C. The high volume fraction of fine Al₃Li precipitates, which depends upon the cooling rate after solidification occurs, makes an important contribution to the as-quenched hardness. A similar distribution of the metastable Al₃Li phase was also precipitated during quenching from the annealing temperature to room temperature but

Al4Li6.5Mg



Al5Li8.5Mg



Al5Li10Mg



Fig. 12 SEM micrographs showing the fracture surfaces of annealed Al-Li-Mg flakes.

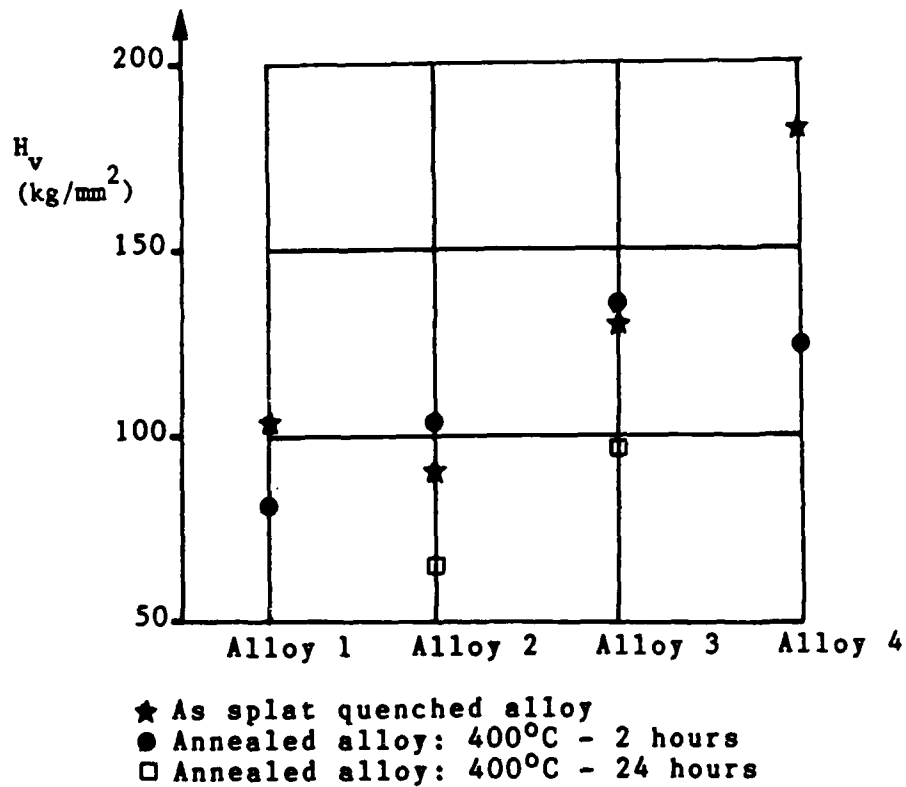


Fig. 13 DPH microhardness of the Al-Li-Mg flakes.

in this case, some of the Li was partitioned to the Al_2LiMg phase and therefore was not available for precipitation as Al_3Li . The volume fraction of the Al_3Li phase as well as its contribution to the hardness is much lower after the annealing treatment than before.

4.3 Study of the Al-Li-Y Flakes

4.3.1 Rapidly-Solidified Microstructure

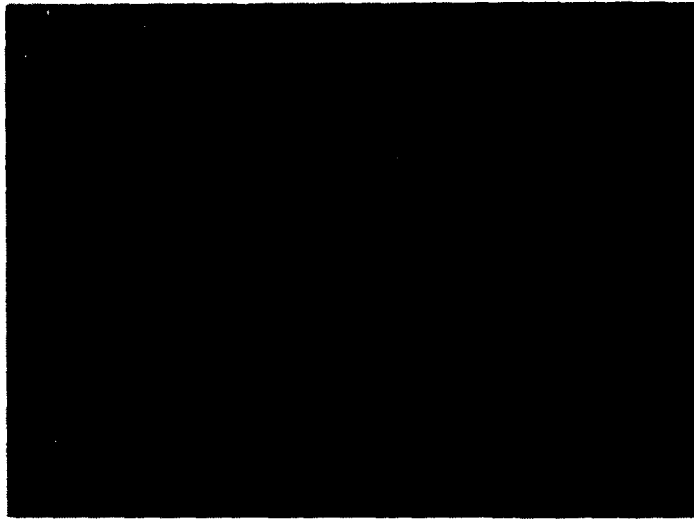
The as-splat quenched microstructure of the Al-Li-Y alloys is similar for both compositions, except for the additional presence of an inhomogeneously distributed coarse primary phase in the thickest flake $\text{Al}_{4.6}\text{Li}_{5.9}\text{Y}$, Figure 14. The cooling rate for this alloy was apparently not high enough to prevent the formation of this constituent phase, which remained stable at an annealing temperature of 300°C . SEM/EDS analysis techniques revealed that much more yttrium is present in this phase than in the aluminum matrix.

The microstructure of the rapidly solidified Al-Li-Y alloys, shown on Figure 15, consists of an Al-rich phase surrounded by a semi-continuous network of an Y-rich phase, as revealed by EDS techniques. The spacing between the Y-rich phase is variable within the same material. The lithium precipitated during rapid quenching as a fine dispersion of metastable Al_3Li precipitates within the Al-phase. X-ray diffraction performed on samples of both alloys gave a similar x-ray ring patterns whose interplanar spacings are listed in the Appendix. The Y-phase(s) were not identified; the x-ray patterns could not be correlated with d-spacings of known phases.

Y-rich phase formed during solidification either by a cellular-type solidification reaction, or prior to Al-matrix solidification as primary particles. It appears that solidification of alloy $\text{Al}_{4.6}\text{Li}_{5.9}\text{Y}$ gave rise to a cellular structure with the yttrium segregated at the cell boundaries in very fine particles, and that alloy $\text{Al}_{4.5}\text{Li}_{9.8}\text{Y}$ solidified according to the second solidification process. Yttrium segregation is enhanced by the diffusion phenomenon. Interdiffusion of lithium and yttrium is impeded by the much lower yttrium diffusivity in aluminum than that of lithium (51,52).

4.3.2 Annealed Microstructure

A two hour annealing treatment of the flakes at 300°C did not result in significant microstructural changes, compare Figure 16 with Figure 14. TEM examination of the annealed foils revealed the presence of Al_3Li precipitates which were finer than those present in the as-solidified alloys, and which gave rise to



Al_{4.6}Li_{5.9}Y

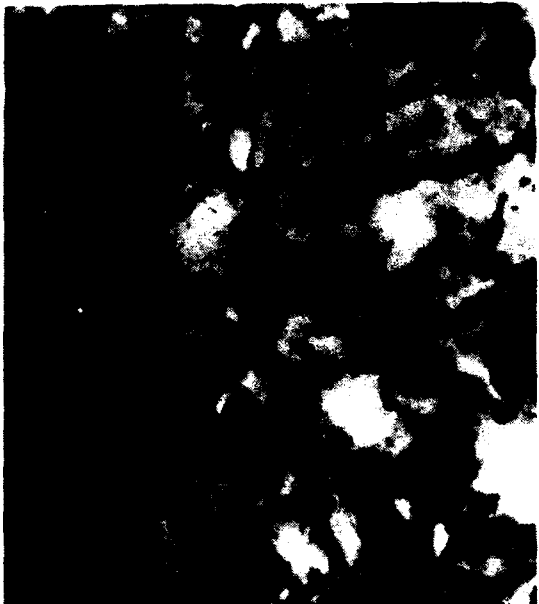


Al_{4.5}Li_{9.8}Mg

Fig. 14 Optical micrographs of as-splat quenched Al-Li-Y flakes.

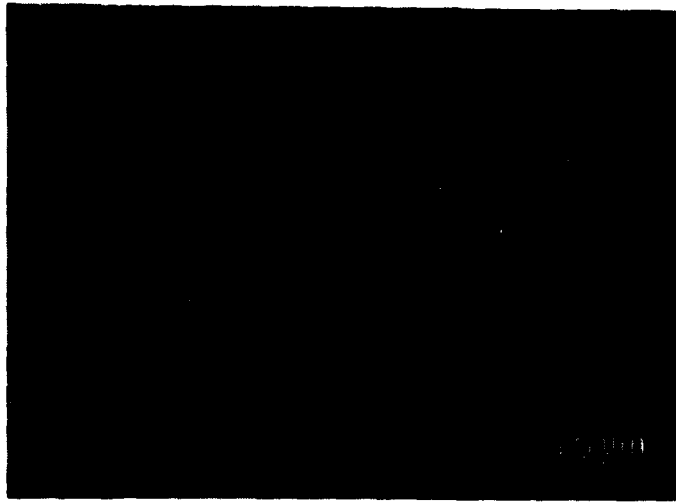


Al_{4.6}Li_{5.9}Mg: two different areas of the same foil

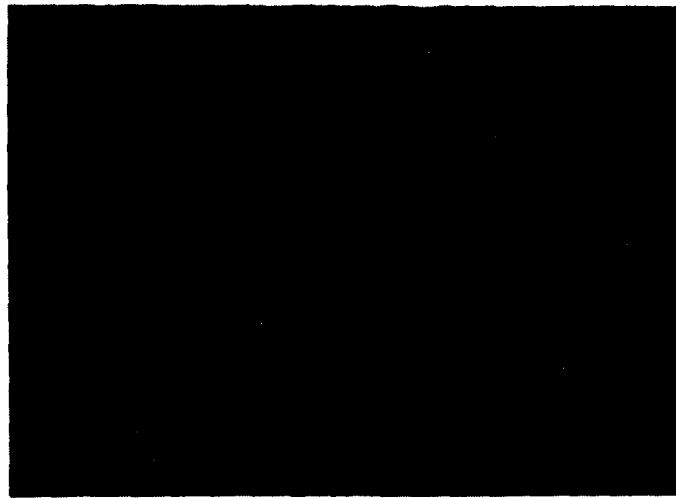


Al_{4.5}Li_{9.8}Y

Fig. 15 TEM micrographs of as-splat quenched Al-Li-Y flakes.



Al_{4.6}Li_{5.9}Y



Al_{4.5}Li_{9.8}Y

Fig. 16 Optical micrographs of Al-Li-Y flakes annealed for 2 hours at 300°C.

very faint superlattice reflections. The Al_3Li phase is thought to have dissolved at the annealing temperature and was re-precipitated during cooling to room temperature. The annealing treatment did not reduce the volume fraction of yttrium-rich phase(s). Yttrium remained segregated, and in the case of alloy $Al_{4.6}Li_{5.9}Y$, precipitated to form additional large intercellular precipitates, Figure 17.

X-ray diffraction performed on annealed samples of the two flakes confirmed that the Y-phase(s) changed crystal structure during the annealing treatment. The two sets of interplanar spacings are listed in Appendix. The Y-phase in annealed alloy $Al_{4.5}Li_{9.8}Y$ was not identified. The x-ray pattern thought to correspond to the intercellular Y containing phase in annealed alloy $Al_{4.6}Li_{5.9}Y$ is characteristic of Al_3Y (hexagonal) phase which has the Mg_3Cd crystal structure (38,39).

Concepts discussed in Section 2-4 suggested that Al-Li-Y alloys might contain a large volume fraction of the $Al_3(Li,Y)$ phase stable in the $L1_2$ crystal structure at temperatures of $300^\circ C$ and above. The microstructural studies of the two Y-containing flakes show that yttrium segregated during rapid solidification; therefore it was not available to substitute for some of the Li and thus to stabilize the Al_3Li phase. Furthermore, the diffusivity of yttrium in aluminum at temperatures of $300^\circ C$ or more is negligible compared to that of lithium as shown in Table 5. Consequently, dissolution of the Y-containing phase and coprecipitation of Li and Y in a stabilized $Al_3(Li,Y)$ phase would be expected to proceed at very slow rate, even if the $Al_3(Li,Y)$ phase is thermodynamically stable. Since Y additions did not successfully stabilize the Al_3Li phase which was the purpose of this study, the Al-Li-Y flakes complex microstructure was not studied further.

Table 5

Diffusion Coefficients in Aluminum (51,52)

X	D_0 (cm^2/s)	Q (kJ/mol)	D at $300^\circ C$ (cm^2/s)
Li	4.5	139.4	9×10^{-13}
Y (Zr)*	728	0.24	8×10^{-20}
Sb	0.09	121.8	7×10^{-13}

* data for Y approximated by the values found for Zr due to lack of data in the literature.



Al_{4.6}Li_{5.9}Y



Al_{4.5}Li_{9.8}Y: two different areas of the same foil

Fig. 17 TEM micrographs of Al-Li-Y flakes annealed for 2 hours at 300°C.

4.4 Study of the Al-Li-Sb flakes

The two different compositions of antimony-containing alloys have similar microstructures. The grain structure formed during rapid cooling remained fine after the annealing treatment at 300°C, compare Figure 18 with Figure 19. A uniform dispersion of Al₃Li precipitates was observed in the as-splat quenched flakes, as well as in many areas of the annealed flakes. The precipitates in the annealed alloys were much finer than in the as-quenched alloys and therefore did not result from coarsening but rather were precipitated upon cooling from 300°C to room temperature.

The equilibrium AlLi phase nucleated mainly heterogeneously during the 300°C annealing treatment. AlLi precipitates can easily be recognized on the TEM micrographs of Figure 19 because of the surrounding interface dislocations (53). This high density of misfit dislocations has been usually accounted for by the semi-coherent Al matrix / AlLi phase interface. Electron diffraction data from AlLi particles were not obtained due to the significant lattice distortion accompanying their presence and also due to the presence of oxides. X-ray diffraction confirmed the presence of the AlLi phase in the annealed alloys. An additional x-ray ring pattern, characteristic of the gamma LiAlO₂ oxide, was found in the as-quenched and annealed alloys. This oxide may only be incorporated in the surface film, or may have entered the melt prior to solidification. No evidence of oxide particles was found within the alloys observed using TEM.

The microstructure of these alloys was not fully understood. The features revealed by optical metallography, Figures 20 and 21, could not be conclusively identified. They may correspond to grain boundary etching effects, to second phase particles (although no evidence of second phase other than AlLi phase was detected by x-ray methods), or to oxide particles. The grain boundary precipitates in the as-splat quenched flake Al_{4.4}Li₁₃Sb as well as the fine particles in the annealed flake Al_{4.5}Li₈Sb were not identified.

EDS techniques performed using the TEM and SEM did not detect the presence of antimony in either alloy. Semi-quantitative analysis was then made on flake Al-4.5Li-8Sb at Kent Laboratories and revealed an antimony level of 0.1 wt%. It is believed that the high vapor pressure of antimony resulted in loss of most of the antimony during melting and solidification, thus accounting for the unexpectedly low Sb content in the alloys.

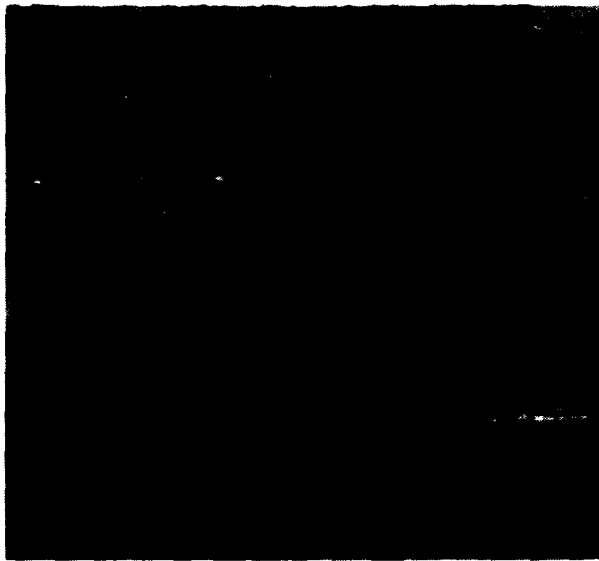


Al_{4.5}Li₈Sb



Al_{4.4}Li₁₃Sb

Fig. 18 TEM micrographs of as-splat quenched Al-Li-Sb flakes.

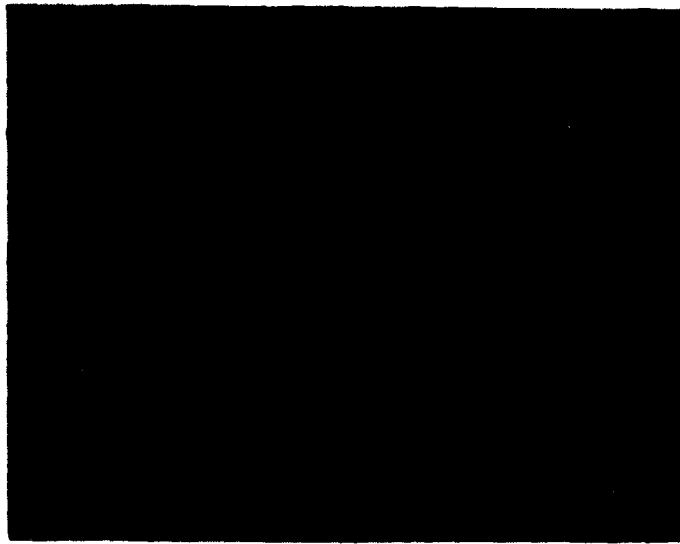


Al_{4.5}Li₈Sb



Al_{4.4}Li₁₃Sb

Fig. 19 TEM micrographs of Al-Li-Sb flakes annealed for 2 hours at 300°C.

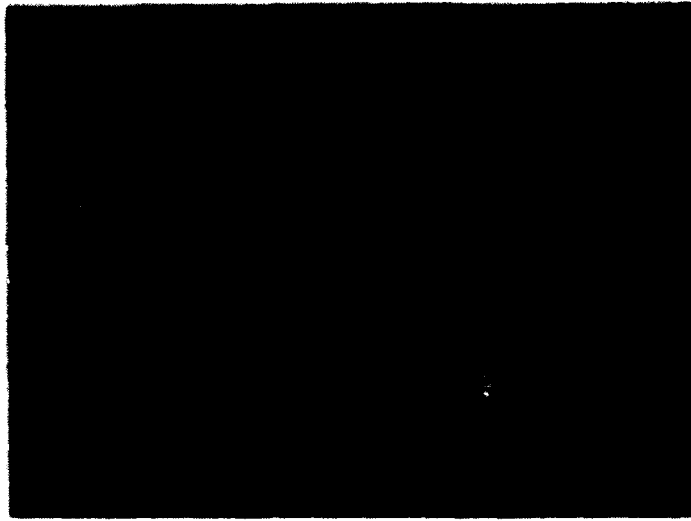


Al_{4.5}Li₈Sb



Al_{4.4}Li₁₃Sb

Fig. 20 Optical micrographs of as-splat quenched Al-Li-Sb flakes.



Flake Al_{4.5}Li₈Sb



Flake Al_{4.4}Li₁₃Sb

Fig. 21 Optical micrographs of Al-Li-Sb flakes annealed for 2 hours at 300°C.

The choice of antimony as a third element was dictated by the same concepts that led to the study of yttrium containing Al-Li alloys (see Section 2-4). The advantage of adding Sb rather than adding Y is that Sb diffuses in aluminum at about the same rate as Li does, as shown by the data of Table 5. The opportunity for stabilizing the Al_3Li phase in an Al-Li-Sb alloy is therefore expected to be greater than in the Al-Li-Y alloys. However, due to the very low Sb content of the rapidly-solidified alloys, stabilization of Al_3Li phase could not be verified and the undesirable AlLi phase was formed during the annealing treatment at 300°C. These alloys were not studied further.

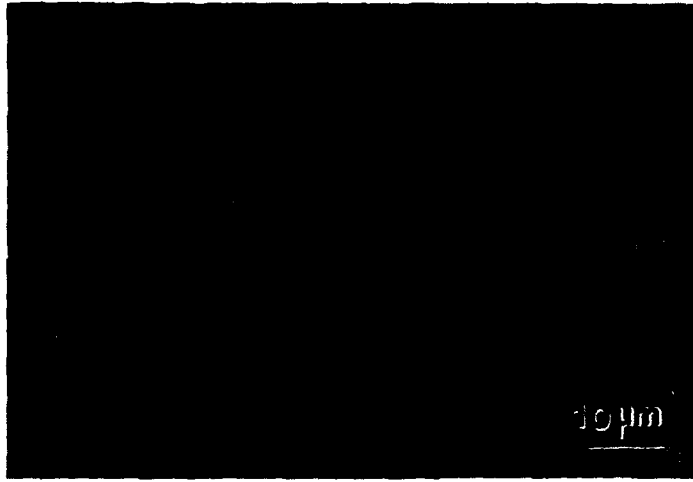
4.5 Microstructure of the Melt-Spun Consolidated Al-Li-Mg Alloy

The microstructure of the melt spun ribbon consists of a fine dispersion of Al_2LiMg particles, detected by x-ray diffraction, which precipitated upon rapid cooling. The 400°C / 2 hour annealing treatment performed on specimens from the ribbon led to coarsening of the Al_2LiMg phase, as shown in Figure 22.

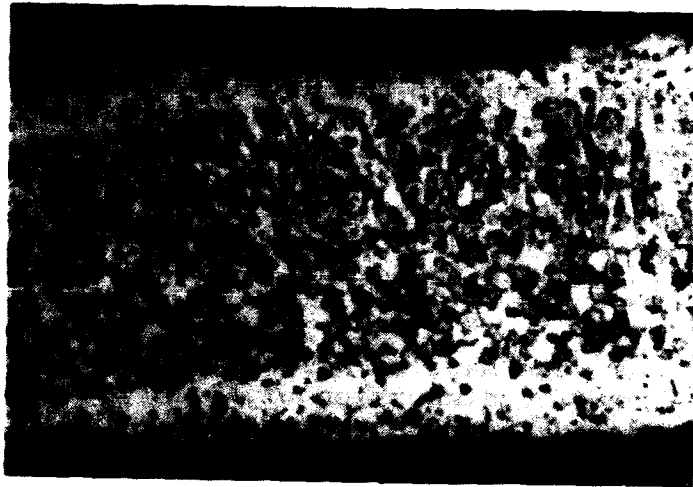
Consolidation of the ribbons induced coarsening of the Al_2LiMg phase in the same manner. The Al_2LiMg phase distribution is similar on the longitudinal, short transverse, and long transverse sections of the as-extruded bar, as shown in Figure 23. The volume fraction of this phase measured on the longitudinal section is 48 volume percent. The high density of oxide particles aligned along prior particle boundaries gives evidence that the oxide layer of the attrited ribbons was not sufficiently broken-up during extrusion, despite the high extrusion ratio used. This is perhaps related to use of a tapered die, which is nearly equivalent to a streamlined die for this type of extrusion. A streamlined die minimizes redundant deformation, an undesirable characteristic for consolidation of PMP aluminum alloys in which the oxide layer cannot be reduced during degassing.

TEM observations were made on a longitudinal section of the extruded material. A fine dispersion of Al_3Li precipitates, similar to that observed in the annealed quenched Al-Li-Mg flakes, is present in the Al-rich phase which corresponds to the bright area of the micrographs of Figure 24. The structure which was developed during extrusion contains 1 to 2 μm grains.

The strength of the extruded material, which consists of 48 volume percent of Al_2LiMg precipitates 1 to 2 μm in diameter, is mainly dictated by matrix work-hardening and by mechanical restraint of the matrix by the precipitates. An applied load would induce a hydrostatic state of stress around the precipitates. The interaction of these stress fields is likely, due to the high volume fraction of the second phase. Therefore, the strength of this material is expected to be high. This explains why the DPH measured on the extruded bar is 195 kg/mm², from which a yield strength near 600 MPa can be estimated.



As-quenched ribbon



Annealed ribbon

Fig. 22 Optical micrographs of Al-5.65Li-9.8Mg melt spun ribbon.

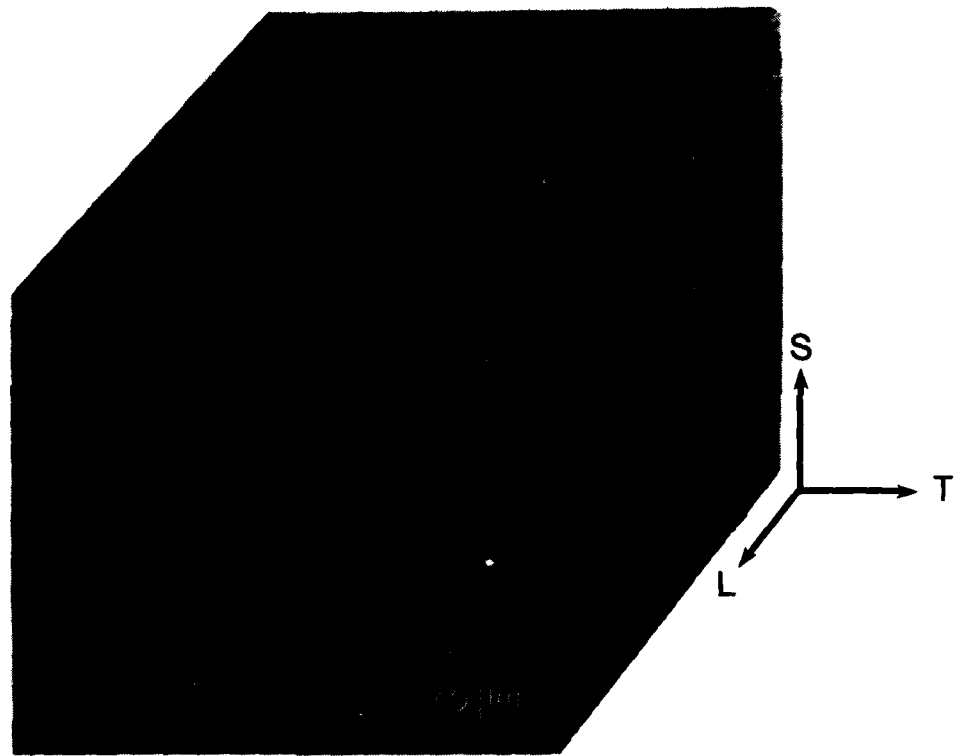


Fig. 23 Optical micrographs showing the L, S and T sections of the Al-5.65Li-9.8Mg extruded bar.

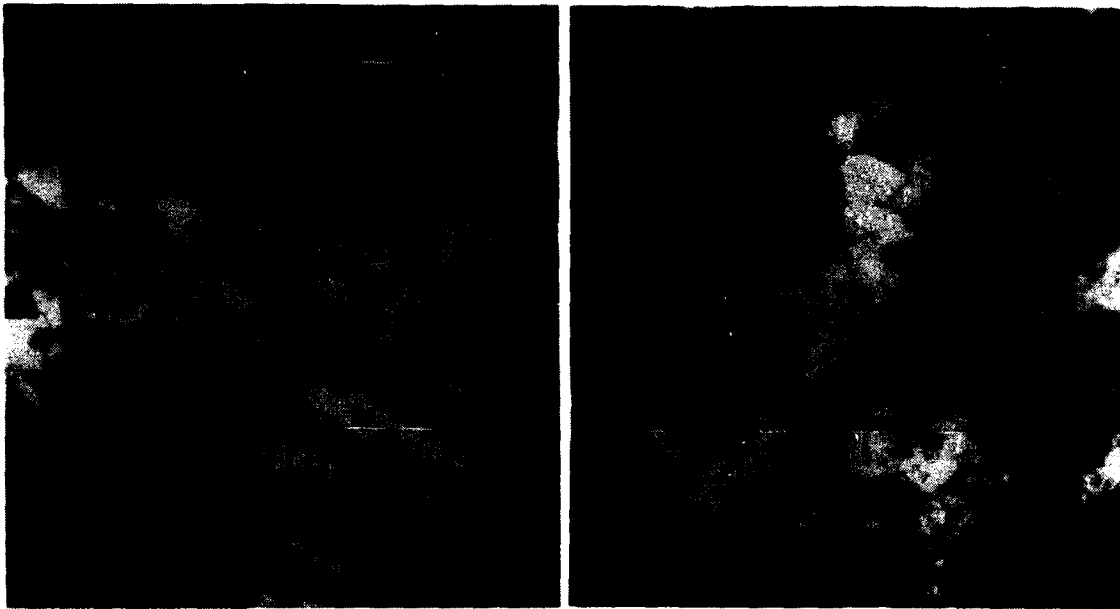


Fig. 24 TEM micrographs showing a longitudinal section of the Al-5.65Li-9.8Mg extruded bar.

5. FUTURE WORK

Future work on this contract will be focused on three topics: production and characterization of an alloy composition with lower levels of Li and Mg, characterization of the mechanical and corrosion properties of the extruded materials, and further examination of the phase equilibria in the Al-Li-Y system. Details of these efforts are presented in the remainder of this section.

The extruded bar containing approximately 48 volume percent Al_2LiMg phase is brittle because the intermetallic phase forms a continuous network through the material. This type of microstructure had been previously observed for the annealed Al5Li10Mg flake, and several factors combined to reproduce this microstructure in the extruded material. The primary factor is the high level of Li in the alloy, which exceeds the target of 5 wt%. In addition, no previous experience with consolidation of Al-Li-Mg alloys containing such high Li and Mg levels was available to indicate the degree of coarsening of the Al_2LiMg phase which would occur during the hot vacuum degassing and extrusion steps. Thus, the volume fraction is high and the microstructure was somewhat coarser than expected. These factors combined to produce a microstructure in which there are easy crack propagation paths. The brittle nature of this alloy indicates that the Li level is too high, and a second alloy composition will be prepared with a lower Li content, near 4.5 wt%.

On the positive side, two characteristics of the first extruded alloy suggest that a reasonable combination of properties may be obtained by the approach we are pursuing. First, the density of the extruded bar is quite low, 2.2 Mg/m^3 . This is 21% lower than the density of 7075 Al, exceeding our target of a 15 to 20% reduction. Second, the yield strength of the material, as deduced from microhardness measurements, is near 600 MPa, somewhat higher than anticipated. Both of these characteristics suggest that we can reduce the Li concentration, still maintaining attractive strength and density, to regain toughness.

Evaluation of the properties of the first extruded bar is now being conducted, although we are unable to perform some tests because of the extremely brittle nature of the material. Tests to measure the yield stress, toughness and corrosion characteristics are being conducted. A more comprehensive set of tests will be conducted on the second extrusion which we expect to exhibit higher toughness.

Finally, the availability of several rapidly-solidified Al-Li-Y alloy compositions provides an opportunity to perform phase relationship studies in this system, which have not previously been reported. This is a relatively small effort, but observations of this type may help us understand why the Al-Li-Y alloys did not produce a stabilized $Al_3(Li,Y)$ phase.

6. REFERENCES

1. D. Webster, in Aluminum-Lithium Alloys, T.H. Sanders, Jr. and E.A. Starke, Jr. (eds), The Metallurgical Society of AIME, Warrendale, 1981, 228-239.
2. E.S. Balmuth and R. Schmidt, in Aluminum-Lithium Alloys, T.H. Sanders, Jr. and E.A. Starke, Jr. (eds), The Metallurgical Society of AIME, Warrendale, 1981, 69-88.
3. W.E. Quist, G.H. Narayanan and A.L. Wingert, in Aluminum-Lithium Alloys II, T.H. Sanders, Jr. and E.A. Starke, Jr. (eds), The Metallurgical Society of AIME, Warrendale, 1984, 313-334.
4. E.A. Starke, Jr., in Sixth International Conference on the Strength of Metals and Alloys, R.C. Gifkins (ed), Pergamon Press, Oxford, 1983, 1025-1044.
5. P. Niskanen, T.H. Sanders, Jr., M. Marek and J.G. Rinker, in Aluminum-Lithium Alloys, T.H. Sanders, Jr. and E.A. Starke, Jr. (eds), The Metallurgical Society of AIME, Warrendale, 1981, 347-376.
6. L. Christodoulou, L. Struble and J.R. Pickens, in Aluminum-Lithium Alloys II, T.H. Sanders, Jr. and E.A. Starke, Jr. (eds), The Metallurgical Society of AIME, Warrendale, 1984, 561-579.
7. A.K. Vasudevan, P.R. Ziman, S.C. Jha and T.H. Sanders, Jr., in Aluminum-Lithium Alloys III, eds C. Baker, P. J. Gregson, S. J Harris, and C. J. Peel, The Institute of Metals, London, 1986, 303-309.
8. A.K. Vasudevan, and T.H. Sanders, Jr., in Aluminum-Lithium Alloys III, eds C. Baker, P. J. Gregson, S. J Harris, and C. J. Peel, The Institute of Metals, London, 1986, 595-601.
9. G.H. Narayanan, J.E. Magnuson, W.E. Quist and A.L. Wingert, "Low Density Aluminum Alloy development," Fifth Interim Technical Report, Air Force Contract F33615-81-C-5053, May 1985.
10. F. H. Froes and J. R. Pickens, Journal of Metals, 36, No.1, 1984, 14-28.
11. F. H. Froes, Y-W. Kim and F. Helmann, Journal of Metals, 39, No.8, 1987, 14-21.
12. N. J. Grant and P.M. Pelloux, in Rapid Solidification Technology Source Book, ed R. L. Ashbrook, American Society for Metals, Metals Park, Ohio, 1983, 361-380.
13. R. E. Maringer, in Rapid Solidification Technology Source Book, ed R. L. Ashbrook, American Society for Metals, Metals Park, Ohio, 1983, 121-128.

NADC 88078-60

14. P. J. Meschter, R. J. Lederich and J. E. O'Neal, in Aluminum-Lithium Alloys III, eds C. Baker, P. J. Gregson, S. J. Harris, and C. J. Peel, The Institute of Metals, London, 1986, 85-96.
15. Y-W. Kim, W. M. Griffith and F. H. Froes, *Journal of Metals*, **37**, No.8, 1985, 27-33.
16. W. M. Griffith, Y-W. Kim and F. H. Froes, in Rapidly Solidified Powder Aluminum Alloys, ASTM STP 890, eds M. E. Fine and E. A. Starke, Jr., American Society for Testing and Materials, Philadelphia, PA, 1986, 283-303.
17. S. W. Ping, in Rapidly Solidified Powder Aluminum Alloys, ASTM STP 890, eds M. E. Fine and E. A. Starke, Jr., American Society for Testing and Materials, Philadelphia, PA, 1986, 369-380.
18. G. S. Koln, *Aluminium*, **60**, No.12, 1984, E768-E773.
19. T. Sheppard, H. B. McShane, M. A. Zaidi and G. H. Tan, *Journal of Mechanical Working Technology*, **8**, 1983, 43-70.
20. G. H. Tan, M. A. Zaidi, and T. Sheppard, *Powder Metallurgy*, **27**, No1, 1984, 3-8.
21. N. J. Kim, D. J. Skinner, K. Okazari and C. M. Adam, in Aluminum-Lithium Alloys III, eds C. Baker, P. J. Gregson, S. J. Harris, and C. J. Peel, The Institute of Metals, London, 1986, 78-84.
22. N. J. Kim, R. L. Bye and S. K. Das, in 4th International Aluminum Lithium Conference, eds G. Champier, B. Dubost, D. Miannay and L. Sabetay, Societe Francaise de Metallurgy, Paris, France, 309-315.
23. G. H. Tan and T. Sheppard, *Powder Metallurgy*, **29**, No2, 143-151.
24. I. G. Palmer, R. E. Lewis and D. D. Crooks, in Aluminum-Lithium Alloys, eds T. H. Sanders, Jr. and E. A. Starke, Jr., The Metallurgical Society of AIME, Warrandale, 1981, 241-262.
25. R. A. Ricks, P. M. Budd, P. J. Goodhew, V. L. Kohler and T. W. Clyne, in Aluminum-Lithium Alloys III, eds C. Baker, P. J. Gregson, S. J. Harris, and C. J. Peel, The Institute of Metals, London, 1986, 97-104.
26. P. J. Meschter, P. S. Pao, R. J. Lederich and J. E. O'Neal, in Rapidly Solidified Powder Aluminum Alloys, ASTM STP 890, eds M. E. Fine and E. A. Starke, Jr., American Society for Testing and Materials, Philadelphia, PA, 1986, 512-526.

27. K. K. Sankaran, S. M. L. Sastry and J. E. O'Neal, in Aluminum-Lithium Alloys, eds T. H. Sanders, Jr. and E. A. Starke, Jr., The Metallurgical Society of AIME, Warrandale, 1981, 189-203.
28. A. Gysler, R. Crooks and E. A. Starke, Jr., in Aluminum-Lithium Alloys, eds T. H. Sanders, Jr. and E. A. Starke, Jr., The Metallurgical Society of AIME, Warrandale, 1981, 263-291.
29. K. K. Sankaran and N. J. Grant, in Aluminum-Lithium Alloys, eds T. H. Sanders, Jr. and E. A. Starke, Jr., The Metallurgical Society of AIME, Warrandale, 1981, 205-227.
30. R. C. A. Pratt, P. Tsakiroopoulos, H. Jones, R. W. Gardiner and J. E. Restall, in 4th International Aluminum Lithium Conference, eds G. Champier, B. Dubost, D. Miannay and L. Sabetay, Societe Francaise de Metallurgy, Paris, France, 341-346.
31. M. S. Mahmoud, H. B. McShane and T. Sheppard, in 4th International Aluminum Lithium Conference, eds G. Champier, B. Dubost, D. Miannay and L. Sabetay, Societe Francaise de Metallurgy, Paris, France, 327-334.
32. A. E. Dwight and P. A. Beck, Transactions of The Metallurgical Society of AIME, 215, 1959, 976-979.
33. P. A. Beck, Advances in X-Ray Analysis, 12, 1969, 1-21.
34. C. T. Liu and J. O. Stiegler, Science, 226, 1984, 636-642.
35. R. E. Watson and L. H. Bennett, J. Phys. Chem. Solids, 39, 1978, 1235-1242.
36. J. H. N. Van Vucht and K. H. J. Buschow, Philips Journal of Research, 19, 1964, 319-322.
37. J. H. N. Van Vucht and K. H. J. Buschow, Journal of Less-Common Metals, 10, 1965, 98-107.
38. D. M. Bailey, Acta Crystallogr., 23, 1967, 729-733.
39. T. Dagerhamn, Arkiv for kemi, 27, 1967, 363-380.
40. H. M. Flower, P. J. Gregson, Materials Science and Technology, 3, 1987, 81-90.
41. F. W. Gayle and J. B. Vandersande, in Aluminum-Lithium Alloys III, eds C. Baker, P. J. Gregson, S. J. Harris, and C. J. Peel, The Institute of Metals, London, 1986, 376-385.
42. F. W. Gayle and J. B. Vandersande, in Rapidly Solidified Powder Aluminum Alloys, ASTM STP 890, eds M. E. Fine and E. A. Starke, Jr., American Society for Testing and Materials, Philadelphia, PA, 1986, 137-153.

43. N. J. Kim, J. M. Howe and E. G. Boden, in 4th International Aluminum Lithium Conference, eds G. Champier, B. Dubost, D. Miannay and L. Sabetay, Societe Francaise de Metallurgy, Paris, France, 457-463.
44. G. E. Thompson and B. Noble, Journal of The Institute of Metals, 101, 1973, 111-115.
45. K. Dinsdale, S. J. Harris and B. Noble, in Aluminum-Lithium Alloys, eds T. H. Sanders, Jr. and E. A. Starke, Jr., The Metallurgical Society of AIME, Warrandale, 1981, 101-118.
46. I. N. Fridlyander, V. F. Shamray and N. V. Shiryayeva, Yzvestiya Akademii nauk SSSR Metall, 2, 1965, 153-158.
47. I. N. Fridlyander, S. M. Ambartsumyan, N. V. Shiryayeva and R. M. Gabidullin, Metal Science and Heat Treatment, 3, 1968, 211-212.
48. S. J. Harris, B. Noble and K. Dinsdale, in Aluminum-Lithium Alloys II, eds T. H. Sanders, Jr. and E. A. Starke, Jr., The Metallurgical Society of AIME, Warrandale, 1984, 219-223.
49. B. Dubost, P. Bompard and I. Ansara, in 4th International Aluminum Lithium Conference, eds G. Champier, B. Dubost, D. Miannay and L. Sabetay, Societe Francaise de Metallurgy, Paris, France, 473-479.
50. D. W. Levinson and D. J. McPherson, Transactions, American Society for Metals, 48, 1956, 689-705.
51. M. Bishop and K. E. Fletcher, The Institute of Metals, 17, 1972, 203-225.
52. L. F. Mondolfo, Aluminum Alloys: Structure and Properties, Butterworths, London, 1979.
53. W.S. Miller, J. White and D.J. Lloyd, in Aluminum Alloys, Their Physical and Mechanical Properties, eds E.A. Starke and T.H. Sanders, Engineering Materials Advisory Services Ltd., West Midlands, U.K., 1986, 1799-1836.

NADC 88078-60

7. APPENDIX

Table A1

X-ray Data for Alloy Al4.6Li5.9Y

As-splat quenched		Annealed	
d(A) *	I/Io	d(A)	I/Io
7.5	w	5.2	m
4.8	w	4.7	w
3.8	s	3.7	s
3.6	w	3.3	s
3.2	w	3.1	s
3.0	m	2.6	s
2.9	m	2.5	m
2.8	w	2.4	s
2.5	s	2.3	Al phase
2.3	Al phase	2.2	s
2.2	m	2.0	Al phase
2.1	m		
2.0	Al phase		

* d: observed interplanar spacing

Table A2

X-ray Data for Alloy Al4.5Li9.8Y

As-splat quenched		Annealed	
d(A)	I/Io	d(A)	I/Io
7.5	m	4.2	m
4.8	m	3.9	w
4.1	w	3.6	s
3.8	s	3.0	m
3.0	m	2.5	m
2.8	w	2.4	m
2.5	s	2.3	Al phase
2.4	w	2.2	m
2.3	Al phase	2.1	w
2.2	w	2.0	Al phase
2.1	w		
2.0	Al phase		

NADC 88078-60

Sandia National Laboratory, Albuquerque, NM 87185,
Div. 1822 and 1832..... 2
TRW, Inc., 23555 Euclid Av., Cleveland, OH 44117..... 1
U.S. Army Air Mobility R&D Laboratory, Fort Eustis,
VA 23064, SAVDL-EU-SS..... 1
United Technologies, Pratt and Whitney, P.O. Box 2691,
West Palm Beach, Fl. 33402, J. Simon Jr..... 1
USAF Systems Command, WPAFB, OH 45331..... 1
University of California, Dept. of Mechanical Engineering,
Irvine, CA 92717, E.J. Lavernia..... 1
University of Virginia, Light Metals Center, Charlottesville,
VA 22901, J. Wert, J. Hawk, E.A Starke, Jr..... 3
Center for Naval Analyses, 4401 Font Ave. P.O. Box 16268
Alexandria, VA 22302-0268..... 1

NADC 88078-60

Martin Marietta Laboratories, 1450 South Rolling Rd.,
 Baltimore, MD 21227-3898, J. Venables..... 1

Material Science Corporation, 1777 Walton Rd., Blue Bell,
 PA 19422..... 1

McDonnell Aircraft Co., Box 516, Saint Louis, MO 63166,
 V.M. Vasey-Glandon and K.K. Sankaran..... 2

MCIC, Battelle Memorial Institute, Columbus OH..... 1

Metcut-Materials Research Group, P.O. Box 33511,
 Wright Patterson AFB, OH 45433, Y.W. Kim..... 1

NASA Headquarters, 600 Independence Av., Washington,
 DC 20546, Mr. N. Mayer..... 1

NASA Langley Research Center, Hampton, VA 23365, A. Taylor..... 1

National Bureau of Standards, Gaithersburg, MD 20899,
 J.R. Manning..... 1

NAVAIRDEVCEN, Warminster, PA, 18974-5000, Library, Code 8131
 (3 Copies), W.E. Frazier, Code 6063 (27 Copies)..... 30

NAVAVNDEP, MCAS, Cherry Point, CA Code 340..... 1

NAVAVNDEP, NAS, Alameda, CA Code 340..... 1

NAVAVNDEP, NAS, Jacksonville, FL Code 340..... 1

NAVAVNDEP, NAS, Norfolk VA Code 340..... 1

NAVAVNDEP, NAS, North Island, CA Code 340..... 1

NAVAVNDEP, NAS, Pensacola, FL Code 340..... 1

NAVAIRSYSCOM, Washington, DC 20361, J. Collins Air-5304,
 L. Slotter Air 931..... 2

NAVAIRTECEN, Patuxent River, MD..... 1

Naval Air Propulsion Test Center, Trenton, NJ 08628,
 R. Mahortor..... 1

Naval Surface Weapons Center, Dahlgren, VA 22448-5000,..... 1

Naval Surface Weapons Center, Silver Spring, MD 20903-5000,
 D. Divecha..... 1

Naval Post Graduate School, Mechanical Engineering
 Department, Monterey, CA 93943, 1

Naval Research Laboratory, Washington, DC 20375, Code 6120,
 Code 6306..... 2

Naval Ship Engineering Center, Washington DC 20360,
 Code 6101E,..... 1

NAVAVNSAFECEN, NAS Norfolk VA, 1

NAVSEASYSYSCOM, Washington, DC 20362..... 1

NAVSHIPRANDCEN, Annapolis, MD 21402..... 1

NAVSHIPRANDCEN, Bethesda, MD 20034..... 1

Northrop, Aircraft Division, One Northrop Av., Hawthorne,
 CA 90250, S.P. Agrawal and G.R. Chanani..... 2

National Science Foundation, Office of Science and
 Technology Centers Division, 1800 G Street, Washington,
 DC 20550..... 1

Office of Naval Research, Washington, DC 20350, S. Fishman
 Code 431..... 1

Office of Naval Technology, Arlington, VA, J. Kelley
 OCNR-225..... 1

Reynolds Metals Co., Fourth and Canal St., P.O. Box 27003,
 D. Thompson..... 1

Rockwell International, Science Center,
 1049 Camino Dos Rios, P.O. Box 1085, Thousand Oaks,
 CA 91360..... 1

NADC 88078-60

NADC-88078-60
Distribution List

	No.
Air Force Wright Aeronautical Lab., Wright Patterson AFB, OH 45433, W. Griffith.....	1
Alcan Rolled Products Co., 100 Erieview Plaza, Cleveland, OH 44114, P. Wakeling.....	1
Alcoa, 1501 Alcoa Building, Pittsburg, PA 15219, F.R. Billman and G.J. Hildeman.....	2
Allied Corp., P.O. Box 1021R, Morristown, NJ 07960, S.K. Das and P. Gilman.....	2
Army Materials and Mechanics Research Center, Watertown, MA....	1
Avco Corp., Applied Technology Divison, Lowell, MA 01851.....	1
Battelle Memorial Institute, Columbus Laboratories, 505 King Av., Columbus, OH 43201.....	1
Boeing Commercial Airplane, Seattle WA , W. Quist.....	1
Boeing Corp., Aerospace Division, P.O. Box 3707, Seattle, WA 98124.....	1
Boeing-Vertol Co., P.O. Box 16858, Phila., PA 19142, Dept. 1951.....	1
British Alcan Aluminum Ltd., Alcan International, Southam Rd., Bambury, Orfordshire OX 167SP, United Kingdom, R. Grines.....	1
Brookhaven National Laboratory, Department of Applied Science/PSD, Building 526, Upton, NY 11973.....	1
Clemson University, Dept. of Mechanical Engineering, Riggs Hall, Clemson, SC 29634-0921, H.J. Rack.....	1
DARPA, 1400 Wilson Blvd., Arlington, VA 22209, B. Wilcox.....	1
Defense Technical Information Center, Cameron Station, Bldg. 5, Alexandria, VA 22314.....	2
Department of Energy, 100 Independence Av., SW Washington, DC 20585, Code CE142.....	1
Drexel University, Dept. of Materials Engineering, 32nd and Chestnut St., Phila., PA 19104, M.J. Koczak.....	1
General Dynamics, Convair Aerospace Division, P.O. Box 748, Fort Wort, TX 76101, Tech. Library.....	1
General Electric Co., Valley Forge Space Center, Phila., PA 19101.....	1
Grumman Areospace Corp., Bethpage, NY 11714, P.N. Adler.....	1
Inco Alloys International, P.O. Box 1958, Huntington, WV 25720, R. Schelleng and R. Benn.....	2
Innovare Inc., Ben Franklin Technology Center, South Mountain Dr., Bethlehem, PA 18015, A.R. Austen.....	1
Kaiser Aluminum, Ravenswood works, Ravenwood, WV 26164, J. M. Hunter.....	1
Lockheed California Co., Burbank, Ca 91520-7631, D.J. Chellman.....	1
Lockheed Missiles and Space Co., Metallurgy Dept. 93-10/204, 3251 Hanover St., Palo Alto CA 94304, R. Lewis and J. Wadworth.....	2
Marko Materials Inc., 144 Rangeway Rd., N. Billerica, MA 01862, R. Ray.....	1